OPTICAL ELECTRON EXCITATION CROSS-SECTION MEASUREMENTS OF THE N_2^+ FIRST NEGATIVE SYSTEM AT ELEVATED TEMPERATURES

J. W. L. Lewis, L. L. Price, and H. M. Powell

ARO, Inc.

June 1973

VON KÁRMÁN GAS DYNAMICS FACILITY
ARNOLD ENGINEERING DEVELOPMENT CENTER
AIR FORCE SYSTEMS COMMAND
ARNOLD AIR FORCE STATION, TENNESSEE

NOTICES

When U. S. Government drawings specifications, or other data are used for any purpose other than a definitely related Government procurement operation, the Government thereby incurs no responsibility nor any obligation whatsoever, and the fact that the Government may have formulated, furnished, or in any way supplied the said drawings, specifications, or other data, is not to be regarded by implication or otherwise, or in any manner licensing the holder or any other person or corporation, or conveying any rights or permission to manufacture, use, or sell any patented invention that may in any way be related thereto.

Qualified users may obtain copies of this report from the Defense Documentation Center.

References to named commercial products in this report are not to be considered in any sense as an endorsement of the product by the United States Air Force or the Government.

OPTICAL ELECTRON EXCITATION CROSS-SECTION MEASUREMENTS OF THE N_2^+ FIRST NEGATIVE SYSTEM AT ELEVATED TEMPERATURES

J. W. L. Lewis, L. L. Price, and H. M. Powell
ARO, Inc.

FOREWORD

The work reported herein was conducted by the Arnold Engineering Development Center (AEDC) under sponsorship of the Air Force Cambridge Research Laboratories (AFCRL) under Program Element 61102F. The AFCRL project monitor was R. O'Neil, who provided the technical objectives of the project.

The results presented were obtained by ARO, Inc. (a subsidiary of Sverdrup & Parcel and Associates, Inc.), contract operator of AEDC, Air Force Systems Command (AFSC), Arnold Air Force Station, Tennessee. The measurements were conducted from May 1971 to May 1972 under ARO Project No. VT0118, and the manuscript was submitted for publication on October 27, 1972.

The authors acknowledge the efforts of C. R. Nelson for fabrication of the gas heater.

This technical report has been reviewed and is approved.

JIMMY W. MULLINS
Lt Colonel, USAF
Chief Air Force Test Director, VKF
Directorate of Test

A. L. COAPMAN
Colonel, USAF
Director of Test

ABSTRACT

Optical electron excitation cross sections of bands of the -2 and -3 sequences of the N_2^+ First Negative System of N_2 were measured over the temperature range from 300 to 900°K. The apparent electron excitation cross sections of the v = 1, 2, 3, and 4 levels, normalized to the v = 0 level, were determined, and enhancement of the experimental values of $\sigma(v \geq 2)$ relative to the predicted values was found for all temperatures investigated. Possible causes of the enhancement and its decrease with increasing temperature are discussed.

CONTENTS

APPENDIXES

I. ILLUSTRATIONS

Figure

Figure Page

II. TABLES

NOMENCLATURE

A	Tube wall area
b	Factor in Eq. (9)
$<c>$	Average molecular speed
D	Nitrogen diffusion coefficient
$E(v')$	Energy eigenvalue of vibrational level v'
E_v^e	Molecular vibrational energy when in equilibrium with surface at temperature T
E_v^f	Molecular vibrational energy following impact with surface at temperature T
E_v^i	Incident molecular vibrational energy before impact with surface at temperature T
e	Electronic charge
h	Planck's constant
I	Electron beam current
i, j	Vibrational quantum numbers
K	Rotational quantum number
k	Boltzmann's constant
M	R-branch upper rotational quantum number
M^{ij}	R-branch upper rotational quantum number of (ij) band at which intensity measurement was cut off
NII	Singly ionized atomic nitrogen
$N_2^+(1-)$	First negative system of ionized molecular nitrogen
$N_2(2+)$	Second positive system of molecular nitrogen
N_2^{K*}	K-shell excitation state of N_2

$N_2^+ B\ ^2\Sigma_u^+$	Upper electronic state of molecular nitrogen ion
$N_2 X\ ^1\Sigma_g^+$	Ground electronic state of nitrogen
$N_2^+ X\ ^2\Sigma_g^+$	Ground electronic state of molecular nitrogen ion
n	Number density of $N_2 X\ ^1\Sigma_g^+$ molecules
$p(vv'')$	Emission band strength for v to v'' $N_2^+(1-)$ transition
$\tilde{p}(vv')$	Excitation band strength for the excitation of level v of $N_2^+ B\ ^2\Sigma_u^+$ from level v' of $N_2 X\ ^1\Sigma_g^+$
Q	Vibrational partition function of the $N_2 X\ ^1\Sigma_g^+$ state
$q(vv'')$	Emission Franck-Condon factor corresponding to $p(vv'')$
$\tilde{q}(vv')$	Excitation Franck-Condon factor corresponding to $\tilde{p}(vv')$
R	Ratio of band intensity ratio at T_V to that at 300°K and defined as $[S(v_1v_1'')/S(v_2v_2'')]_{T_V}/[S(v_1v_1'')/S(v_2v_2'')]_{300°K}$
R_T	Tube radius
$R_e^2[\bar{r}(vv'')]$	Square of the electronic transition moment
$\bar{r}(vv'')$	r-centroid of the v to v'' transition
$S(vv'')$	Intensity of (vv'') vibrational band of $N_2^+(1-)$ system
$S(vv'')_{Exp}$	Experimental value of $S(vv'')$
T	Temperature, °K
T_R	Rotational temperature
T_v	Vibrational temperature
t_c	Average molecular residence time within chamber

t_T	Average molecular residence time within tube
v	Vibrational quantum number of the $N_2^+ B\ ^2\Sigma_u^+$ state
v′	Vibrational quantum number of the $N_2 X\ ^1\Sigma_g^+$ state
v′′	Vibrational quantum number of the $N_2^+ X\ ^2\Sigma_g^+$ state
x	Radial distance within tube
Z_{01}	Average number of gas phase collisions required for vibrational excitation of the v = 1 level of N_2 molecules
Z_{10}	Average number of gas phase collisions required for vibrational deactivation of N_2 molecules of v = 1
Z_s	Average number of collisions of a molecule with the surface of the capillary tube
α^{ij}	Fractional intensity of (ij) band for $M > M^{ij}$
α_v	Vibrational energy accommodation coefficient
$\beta(N_2^{K*}v)$	Branching factor
$\Gamma(v)$	Enhancement ratio of $N_2^+ B\ ^2\Sigma_u^+(v)$ radiation, defined as $[\sigma(v)/\sigma(0)]_{Exp}/[\sigma(v)/\sigma(0)]_{Theoretical}$
$\Gamma(v)_{calc}$	Enhancement ratio using $[\sigma(v)/\sigma(0)]_{Exp}$ in place of $[\sigma(v)/\sigma(0)]_{Theoretical}$ with scaled excitation Franck-Condon factors
$\Gamma(vv'')$	Enhancement ratio of $N_2^+ B\ ^2\Sigma_u^+(vv'')$ radiation and defined as $[\sigma(vv'')/\sigma(00)]_{Exp}/[\sigma(vv'')/\sigma(00)]_{Theoretical}$
$\lambda(vv'')$	Wavelength of the v to v′′ transition
ν	Vibrational frequency of nitrogen
$\sigma(N_2^{K*})$	Excitation cross section of N_2^{K*} state
$\sigma(v)$	Apparent electron excitation cross section of vibrational state v

$\sigma(vv'')$	Optical electron excitation cross section for the v to v'' transition
$\sigma'(v)$	Apparent cross section of excitation attributable to Auger decay, equal to $\sigma(N_2^{K*})\beta(N_2^{K*}, v)$
$\tau(v)$	Lifetime of vibrational level v of $N_2^+ B\ ^2\Sigma_u^+$ state

SECTION I
INTRODUCTION

1.1 BACKGROUND

The electron beam fluorescence technique has been used with qualified success during the past decade for measurements of density as well as rotational and vibrational temperatures of nitrogen in hypersonic aerodynamic simulation facilities. As is described in detail in the following sections, the impact of high-energy electrons with N_2 molecules produces, among other electronic systems, the $N_2^+(1-)$ electronic transition system. Typical past applications of this technique in conducting vibrational temperature measurements have used vibrational bands originating from the vibrational levels v = 0, 1, and 2 of the upper state $B\,^2\Sigma_u^+$. Consistent with this selection of vibrational bands, the statement is usually made that the electron beam fluorescence technique is capable of T_v measurements for $T_v \gtrsim 800°K$. However, if transitions of the $N_2^+(1-)$ system originating in vibrational levels $v \geq 3$ are observed, it will be seen that measurements of T_v as low as approximately 500°K are feasible, insofar as temperature sensitivity is concerned. The primary requirements for extension of the technique to measurements of T_v as low as 500°K are sufficient sensitivity of the detection system and accuracy of the excitation model.

The desirability for such an extension of the technique has been prompted primarily by the potential offered by the utilization of rocket-borne electron beam systems for atmospheric measurements (Ref. 1). Such measurements include, in the first instance, altitude profile determinations of density, rotational temperature, T_R, and vibrational temperature, T_v, of N_2 over the 90- to 200-km altitude range, and the results find applicability in the understanding of such problems as atmospheric chemistry, auroral phenomena, and atmospheric turbulence and gravity waves (Ref. 2). The present study was initiated for the purpose of investigating the validity of the model of the $N_2 X\,^1\Sigma_g^+ \rightarrow N_2^+ B\,^2\Sigma_u^+$ excitation-ionization process over the temperature range from 300 to 1000°K. Specifically, measurements of the $\Delta v = -2$ and -3 sequences of the $N_2^+(1-)$ system were obtained over the just-mentioned temperature range, and comparisons with theoretical predictions were performed.

1.2 ELECTRON BEAM EXCITATION-EMISSION EQUATIONS

The excitation-emission equations are sufficiently well known so that only a summary of the excitation-emission model will be presented along with the resulting theoretical equations.

Electron beam-induced changes in the rotational quantum number, K, for the excitation of the $N_2^+B\ ^2\Sigma$ state are assumed to be $\Delta K = \pm 1$; i.e., only dipole excitations in rotation are allowed. It can easily be shown that the vibrational band intensity, $S(vv'')$, describing the photon emission rate per unit length of the electron beam for the electronic transition $N_2^+B\ ^2\Sigma_u^+(v) \rightarrow N_2^+X\ ^2\Sigma_g^+(v'')$ can be written as

$$S(vv'') = \frac{I}{e} \times n \times \sigma(vv'') \tag{1}$$

where $\sigma(vv'')$ is defined as the optical electron excitation cross section for the v to v'' transition of the $N_2^+(1-)$ system. It is also known that the optical cross section, $\sigma(vv'')$, can be written in terms of the lifetime, $\tau(v)$, of level v, emission band strength, $p(vv'')$, and excitation band strength, $\tilde{p}(vv')$, as

$$\sigma(vv'') = [p(vv'')\tau(v)/\lambda^3(vv'')] \times \sum_{v'} \tilde{p}(vv') \exp\left[\frac{-E(v')}{kT_v}\right]/Q \tag{2}$$

where Q = vibrational partition function of the $N_2X\ ^1\Sigma_g^+$ state, $E(v')$ = energy eigenvalue of level v' of the $N_2X\ ^1\Sigma_g^+$ state, and $\lambda(vv'')$ = transition wavelength. From the definition of the lifetime, $\tau(v)$, it is seen that the apparent excitation cross section, $\sigma(v)$, can be written as

$$\sigma(v) = \sum_{v''} \sigma(vv'') = \sum_{v'} \tilde{p}(vv') \exp[-E(v')/kT_v]/Q \tag{3}$$

The ratio of the vibrational band intensities $S(v_1v_1'')$ and $S(v_2v_2'')$ can be written as

$$S(v_1v_1'')/S(v_2v_2'') = \sigma(v_1v_1'')/\sigma(v_2v_2'') = [p(v_1v_1'')/p(v_2v_2'')] \times [\tau(v_1)/\tau(v_2)] \times [\lambda(v_2v_2'')/\lambda(v_1v_1'')]^3 \times [\sigma(v_1)/\sigma(v_2)] \tag{4}$$

It is noted that sufficiently low gas density values are assumed to preclude collisional quenching correction terms to the above equations. Additionally, it may be seen that the entire temperature dependence of Eq. (4) is contained within the ratio of cross sections $\sigma(v_1)/\sigma(v_2)$.

The fact is recalled that the vibrational band strength, $p(vv'')$, is related to the corresponding Franck-Condon factor, $q(vv'')$, and the square of the electronic transition moment, $R_e^2[\bar{r}(vv'')]$, by

$$p(vv'') = q(vv'') R_e^2[\bar{r}(vv'')] \tag{5}$$

where $\bar{r}(vv'')$ is the r-centroid of the transition. The set of emission band strengths was determined using the unpublished data and calculations of Williams, Hornkohl, and Lewis (Ref. 3) and the data of Wallace and Nicholls (Ref. 4). Both emission and excitation Franck-Condon factors as well as r-centroids were provided by J. O. Hornkohl of ARO, Inc., and Tables Ia and b, Appendix II, list these parameters.

Values of the lifetime, $\tau(v)$, for the levels v = 0, 1, 2, 3, and 4 of the $N_2^+ B\,^2\Sigma$ state were calculated using the expression

$$\tau(v) = \left[\Sigma_{v''} p(vv'')/\lambda^3(vv'')\right]^{-1} \tag{6}$$

and the bandhead wavelength values of Tyte and Nichols (Ref. 5). The value of $\tau(0) = 6.58 \times 10^{-8}$ sec of Bennett and Dalby (Ref. 6) was used for normalization. The resulting values are shown in Table II. Also shown in Table II are the values of $\tau(v)$ obtained using Franck-Condon factors rather than band strengths. Since no excitation band strength data exist, excitation Franck-Condon factors, $\tilde{q}(vv')$, are used in their stead.

Using the values of $p(vv'')$, $\tilde{q}(vv')$, and $\tau(v)$ obtained using emission band strengths, the ratios $\sigma(v_1v_1'')/\sigma(v_2v_2'') = S(v_1v_1'')/S(v_2v_2'')$ of various bands of the $\Delta v = -2$ and -3 sequences were calculated using Eqs. (3) and (4). Figures 1 and 2, Appendix I, show the variation with T_v of the ratios S(13)/S(02), S(24)/S(02), S(35)/S(02), S(46)/S(02), S(14)/S(03), S(25)/S(03), S(36)/S(03), and S(47)/S(03). It is obvious from these figures that the sensitivity of the intensity ratio with respect to T_v increases as v increases from 1 to 4, and measurements of T_v are indeed possible for T_v as low as approximately 500°K if bands are used

for which $v \geq 3$. The only qualifications of this statement are the requirement of sufficient detection sensitivity and the accuracy of the excitation model. Figures 3 and 4 show the variation with T_v of the above ratios when normalized to their room temperature values,

$$R = \frac{[S(v_1 v_1'')/S(v_2 v_2'')]_{T_v}}{[S(v_1 v_1'')/S(v_2 v_2'')]_{300^\circ K}}$$

and the temperature sensitivity of each is clearly observed.

1.3 PREVIOUS MEASUREMENTS

Experimental studies of the excitation and emission of the $N_2^+(1-)$ system are many and can be categorized as either excitation cross-section measurements, emission band strength measurements, such as Ref. 4, or utilization of the $N_2^+(1-)$ system for T_v and density measurements (Ref. 3). Neither the second nor the third category of measurements provides direct verification of the excitation model, for the second type requires no knowledge of the excitation mechanism, and the third type presumes its accuracy. Of the first category the most recent and extensive is that of Stanton and St. John (Ref. 7). The measurement of Ref. 7 was conducted at approximately room temperature, and it may be seen that the ratio $S(v_1 v_1'')/S(v_2 v_2'') = \sigma(v_1 v_1'')/\sigma(v_2 v_2'')$ can be approximated by

$$S(v_1 v_1'')/S(v_2 v_2'') \cong [p(v_1 v_1'')/p(v_2 v_2'')] \times [r(v_1)/r(v_2)] \times [\lambda(v_2 v_2'')/\lambda(v_1 v_1'')]^3 \times \bar{p}(v_1 0)/\bar{p}(v_2 0) \quad (7)$$

Consequently, a measurement of $S(v_1 v_1'')/S(v_2 v_2'')$ at room temperature is essentially a measurement of $\tilde{p}(v_1\ 0)/\tilde{p}(v_2 0)$ which, according to Eq. (5), equals $\tilde{q}(v_1\ 0)/\tilde{q}(v_2\ 0)$ if the electronic transition moment is constant with respect to the excitation r-centroid. Table III shows the experimental data of $S(vv'')/S(00)$ reported by Stanton and St. John. It also shows the values of $S(vv'')/S(00)$ calculated from Eq. (4) using both the band strengths and Franck-Condon factors of Table I. The latter calculations are of interest since Stanton and St. John used similar calculations to obtain apparent excitation cross sections of incompletely observed progressions. It should be noted that the data of Ref. 7 shown in Table III exhibit anomalously large ratios for $v \geq 2$, the discrepancies greatly exceeding the experimental imprecision.

The present measurements of the $N_2^+(1-)$ system were confined to the $\Delta v = -2$ and -3 sequences for the purpose of extending the measurements of Stanton and St. John at room temperature and acquiring data at elevated temperatures in order to provide additional verification studies of the excitation model.

SECTION II
EXPERIMENTAL APPARATUS

2.1 EXCITATION CHAMBER AND GAS SUPPLY

For the purpose of providing gas samples at elevated temperatures, a scattering chamber was constructed with an interior cylindrical cooling liner and innermost heater, the chamber, lines, and heater all being aligned both coaxially and horizontally. The outer chamber was a stainless steel cylinder 46 cm long and 28 cm in outer diameter, with a quartz optics port. The water-cooled, copper cylindrical cooling liner extended the length of the outer chamber and, in the radial direction, was situated immediately adjacent to the interior wall of the outer chamber. Its cooling effect maintained the outer chamber wall at sufficiently low temperatures to prevent failure of O-rings used for vacuum sealing of the diffusion pump to the outer chamber. The cooling liner had three 2.5-cm access holes; two were used for optical viewing ports, and one was used for electron beam injection.

Inside of the water-cooled liner was the heater. Its body was a cylindrical steel shell 28 cm long and 11 cm in diameter. Two 15-cm-diam steel flanges with centrally located 1.3-cm-diam holes capped the heater ends. Sixteen 30-cm-long, 95-mm-diam ceramic rods were mounted outside the heater body and coaxial with it, with their ends through evenly spaced flange holes. The heater element was nine turns of 1.3-cm-wide Nichrome® ribbon which was non-inductively wound along the cylindrical axis. The Nichrome ribbon was tied to the rods and was about 6 mm from the body exterior. The observation volume was located, therefore, inside a smooth-walled cylinder having indirectly heated walls. Holes of 1.3-cm and 1.9-cm diameters allowed for the electron beam entrance and exit, respectively, and two slits, each of which was 6 mm wide and 50 mm long and aligned lengthwise parallel to the electron beam, provided optical access. An alternating current (a-c) of 40 amp at approximately 2 kw was required to heat the gas to

temperatures of nearly 1000°K. Five thermocouples were attached to the inside wall of the heater, allowing continuous monitoring of the spatial gradients of the heater temperature. At 1000°K the axial temperature gradients were approximately ±2 percent. Figure 5 is a cutaway schematic of the heater and water-cooled liner.

Chamber pumping was provided by a 6-in. oil diffusion pump with water-cooled baffle, yielding pressures less than 10^{-5} torr. Chamber leak rates were about 10^{-4} torr/min. Since the heater was directly between the gas inlet and pump throat, a gross unidirectional flow through the heater existed. Chamber pressure was controlled by varying the mass flow rate through the system by varying the gate valve opening to the 6-in. diffusion pump. An NRC Alphatron® gage monitored the pressure at a point between the copper liner and chamber wall. The gage was recently calibrated with nitrogen (N_2) and found to be linear over the 10^{-2} to 10^{-1} torr range with an inaccuracy of ±1 percent.

Even though the heated chamber temperature is defined by the thermocouple measurements and, as will be discussed later, the rotational temperature of N_2 is measured, these data alone are insufficient to determine the vibrational temperature of the gas sample. The initial $\Delta v = -2$ study was performed using only the main heater chamber and required that the injected, slowly flowing gas sample impact upon the heated chamber before entering the collision volume. The residence time of the gas sample was estimated to be in excess of 50 sec. Calculations of the gas phase vibrational collision number were performed for N_2 using the simplified Landau-Teller $T^{-1/3}$ dependence of Z_{10}, and the conclusion was that Z_{01} was sufficiently small at temperatures above approximately 750°K to ensure equilibration of the vibrational mode. Of course, although Z_{01} is quite large at 300°K, no change in vibrational energy was required. However, at 600°K the collision number Z_{01} was sufficiently large to render the gas flow system design marginal. The later $\Delta v = -3$ study had incorporated a gas preheater system to ensure vibrational equilibrium at 600°K. Also installed were a volume flow gage and a Wallace and Tiernan pressure gage to provide estimates of the mass flow rate. The preheater system was constructed of a stainless steel capillary tube of 1.3-mm outer diameter and 0.165-mm wall thickness, the smallest diameter tubing on hand. The tubing length was approximately 50 cm, and twelve turns of the tube were wound on a 1.9-cm-diam ceramic core located in the interior of the chamber. The end of the tube located within the chamber was sealed and electrically grounded. For the gas outlet a small hole of approximately 0.2- to 0.5-mm diameter was filed through near its end. The other end of the capillary was

passed through an insulated feed-through flange and connected to the flowmeter and gas supply. Connections to an auxiliary power supply were made externally, and 4 amps ac were required to heat the capillary to approximately 1000°K. A thermocouple was used to monitor the temperature of the capillary.

Using the preheating system in conjunction with the main heater system, typical operating conditions provided a gas flow rate of approximately 5 μg/sec, which yielded a main chamber residence time, t_c, of between 10 and 100 sec. Since the Knudsen number of the flow within the collision chamber is approximately 10^{-2}, gas phase collisions predominate within the collision chamber. Within the capillary tube the average residence time of a molecule, t_T, is between 0.1 and 1 sec, and the capillary Knudsen number, based on the inner diameter, is approximately 1; thus, the flow field is transitional, and, as a result, wall collisions are significant.

Using the relation

$$Z_s/n = t_T\langle c\rangle \times A/4$$

for the average number of collisions of a molecule with the wall of the tubing for t_T = 0.1 sec, one finds Z_S/n to be on the order of 10^5. One may also define the vibrational energy accommodation coefficient, α_V, as

$$a_v = (E_v^f - E_v^i)/(E_v^e - E_v^i)$$

where

E_v^i = incident vibrational energy of a molecule before impact with the surface of temperature T,

E_v^f = vibrational energy following impact,

and

E_v^e = vibrational energy of a molecule if in equilibrium with the surface at temperature T.

Using the expression

$$E_v = h\nu[\exp(h\nu/kT_v)-1]^{-1}$$

where ν is the vibrational frequency of N_2, it can be shown that, since E_v^i is evaluated at 300°K, for E_v^e corresponding to T_v = 550°K,

$$\Delta E_v / E_v^e = (E_v^f - E_v^i)/E_v^e = \alpha_v$$

or

$$\Delta E_v = \alpha_v E_v^e$$

Therefore, if $\alpha_v \simeq 0.2$ for surface collisions, which is considered as a reasonable assumption, then

$$\Delta E_v / E_v^e \simeq 0.2$$

This simply means that from five to ten collisions are required for equilibration. Since it has just been shown that approximately 10^5 collisions with the capillary occur, one now has assurance that equilibrium in the vibrational mode is achieved.

Additional qualitative support to the above argument is provided by considering the passage of a molecule through the tube as a random-walk problem and showing the rms deviation $(\overline{x^2})^{1/2}$ from the tube centerline to be greater than the tube radius, R_T. It is known that

$$\overline{x^2} = 2Dt_T$$

where the N_2 diffusion coefficient, D, was taken to be 0.25 cm^2/sec. This yields, using t_T = 0.1 sec,

$$(\overline{x^2})^{1/2} = 0.2 \text{ cm} > R_T = 0.05 \text{ cm}$$

thereby showing once again a multicollision process with the tube wall.

2.2 ELECTRON GUN SYSTEM

The electron gun system was the same as that reported in Ref. 3. The television (TV)-type electron gun had an oxide-coated cathode and typically provided a steady 1-ma current for 8 hr. A Universal Voltronics high voltage power supply provided a ripple-filtered potential of 10 kv

to the electron gun. Magnetic coils situated near the cathode provided for electron beam focus and deflection upon the 1.3-mm-diam orifice, which was situated about 56 cm from the gun cathode and level with the top of the chamber. A 4-in oil diffusion pump with water-cooled baffle kept this drift tube section at a pressure of 2×10^{-5} torr when the chamber pressure was 3×10^{-2} torr.

Because of space limitations between the heater and water-cooled shell, a flat copper plate inclined at a small angle to the incident beam had to serve as a beam collector. A collector cup with grids would have been preferable for the suppression of secondary electrons. It is felt that use of the small angle of inclination decreased the likelihood of secondary electrons re-entering the collision volume, as the recent work of Schweiger et al. (Ref. 8) demonstrates.

Consequently, the primary deficiency of the flat plate collector is the small inaccuracy in the measured value of the current. The milliammeter was calibrated over the 10- to 1000-μamp range and was found to have an inaccuracy of less than ± 2 percent.

It was observed that the noninductive winding of the heater was less than perfect and that beam spreading resulted. That the direction of spreading was along the line of sight may easily be seen by considering the Lorentz force acting on an electron beam moving diametrally in an axially directed solenoid field. To evaluate the magnitude of the spreading of the beam, a 4.7-mm stainless steel tube was positioned at the center of an insulated flange directly opposite the center of the spectrometer entrance slit. A Swagelok® fitting was modified with an O-ring seat to provide both a linear and a rotary motion vacuum feedthrough, and an external connection to the milliammeter was made. The tube was moved across the heater chamber, and the cumulative electron beam profile was measured for various values of heater current. It was found that spreading along the line of sight was negligible for all temperatures of operation except 900°K and higher. For these highest heater currents, spreading of the beam is sufficiently large to enable as much as 4 percent of the current to be lost to the collector plate at the exit port of the heater chamber. Spreading of the beam along the axial direction was verified to be negligible by rotating the collector tube and measuring the cumulative axial profile with a small rectangular copper strip welded to the underside of the collector tube. It should be noted that the external end of the 4.7-mm tube was connected to a thermocouple pressure gage and that the internal end was open to allow pressure measurements of the heated gas at the center of the heated chamber. As was

expected, the pressure readings were time-dependent immediately after insertion into the heated gas chamber. The initial pressure measurement, together with the gas temperature, provided values of gas number density in approximate agreement with the Alphatron results. Additionally, the final pressure values were approximately corrected for thermal transpiration effects, and, as before, the resulting number density was in approximate agreement with the Alphatron measurement.

2.3 OPTICS AND DETECTOR

A plan view of the $\Delta v = -2$ sequence study apparatus and optical arrangement is shown in Fig. 6. The 5-cm-diam quartz lens employed had a focal length of 100 mm. The overall optical magnification was 1.0, and the spectrometer slit image was parallel with the electron beam. In the $\Delta v = -3$ sequence study, Fig. 7, two glass lenses of 280-mm and 220-mm focal lengths apertured at 2.5 cm were employed. They were positioned at their focal lengths, providing a parallel light path between them in which the neutral density filter and dove prism could be placed. The overall optical magnification was 0.79. A 0.75-m Spex scanning spectrometer was employed with a 1200-groove/mm grating blazed at 3000 Å. The reciprocal linear dispersion was 11 Å/mm. Calibrations of both wavelength and scanning speed were performed.

An EMI 6256 S photomultiplier tube of S-11 spectral response was used with gaseous N_2 cooling. Operating voltage for the tube was 1500 v and was supplied by a Calibration Standards Corporation power supply. Photomultiplier tube temperature was maintained at -20°C, at which temperature the signal-to-noise ratio of the tube was found to be insensitive to temperature fluctuations.

Linearity of the detector with radiation intensity was verified by observing the variation of the $N_2^+(1-)(0,0)$ band with collector beam current. A calibration of the variation of the signal output with slit width setting was performed.

The spectral sensitivity of the overall system was determined using a GE 30A-T24-17 calibrated tungsten strip lamp and an EGG Model 590-11A lamp power supply. For the optical configuration employed in the $\Delta v = -2$ sequence study, the system output was recorded using a

calibrated strip chart recorder. Conversion to units appropriate for photon counting acquisition was performed, and Fig. 8 shows the normalized spectral sensitivity of the system. A change in the optical configuration for the $\Delta v = -3$ sequence study required an additional calibration. Since the method of data acquisition also changed for the $\Delta v = -3$ sequence study, as is explained in following sections, the calibrated strip lamp output was reduced using a 3.0 neutral density filter whose transmission was measured as 0.00143 ±3 percent over the spectral range from 4000 to 5200 Å. The normalized spectral sensitivity of the system for the $\Delta v = -3$ sequence is shown in Fig. 9.

2.4 ELECTRONICS AND DATA ACQUISITION SYSTEM

The data of both the $\Delta v = -2$ and -3 studies were acquired using photon counting detection. However, data recording for the initial $\Delta v = -2$ study was partially digital and partially analog. Later improvements in the recording of the data of the $\Delta v = -3$ study were incorporated to allow solely digital data acquisition, thereby improving accuracy and decreasing acquisition time.

2.4.1 Photon Counting System

The experimental system used the following ORTEC apparatus: Model 454 Timing Filter Amplifier, Model 436 100-MHz Discriminator, and Model 715 Dual Counter/Timer. Figure 10 shows a block diagram of the system.

The 715 counter/timer includes dual counters, one of which, in conjunction with a precise internal oscillator, may be preset for an accurate counting interval so that the system can be used as a discrete rate meter. The amplifier output is negative and passively shaped, depending upon time constant selections. The discriminator provides either positive or negative pulses. Only for applications of extreme pulse rates is the negative output required. The positive pulse is a standardized pulse of +5 v and 0.5 μsec width. The 715 counter has a frequency response of 20 MHz and an approximate dead-time of 50 nsec. The counter/timer will accept either discriminator output, and for the purposes of this report both were usable for the measurements that were made.

2.4.2 Data Recording and Logging System

Several modes of operation were used during the course of the measurements. The initial study of the $\Delta v = -2$ sequence used an accumulated count which was recorded manually at timed intervals while the bands were continuously scanned at about 3 Å/min. Rotational temperature measurements were from resolved line intensities of the strong N_2^+ (1-)(0, 0) band. An analog output for the rotational temperature measurements was obtained through a waveshaping and filtering scheme of the discriminator output and recorded on a strip chart recorder. To accomplish this, a Tektronix oscilloscope was used as a variable pulse stretcher by utilizing the 25-v square pulse gate output, which is of the same width as the sweep. The gate output was applied to an RC filter circuit as shown in Fig. 11. The adjustable pulse width was selected by observing the display and assuring that only one pulse was present on any given sweep. Maximum pulse width without loss of pulses was thereby secured. An alternate, easier, and probably preferable method was to use the system conventionally but to use the timer on external input as a counter. The gate pulse width should be decreased until the dual counters agree on any given preset interval. This assures that the filter is "seeing" all the pulses. Obviously, this should be done for the most intense line on any given scan. The use of this technique requires that the gate width, filter time constant, and scanning speed be compatible. A 3-sec time constant and a 1-Å/min scan rate were used.

For the $\Delta v = -3$ study a scan rate of 4.5 Å/min was used. An alternate recording method utilizing a data logger was incorporated into the measurements in order to improve accuracy, reduce scan times, and afford access to a computer for data reduction purposes. The data logger included a scanner for analog inputs, digital voltmeter, paper tape punch, strip printer, and manual time and point number inputs. Chamber pressure, beam current, and counter readings were recorded every 10 sec. A block diagram of this system is shown in Fig. 12.

Since the data logger had no provision for digital inputs, an interface, which is referred to as a Counter Readout Control (CRC) module, was required to accept digital output from the counters and provide an analog input to the logger. Although this is not the most efficient means of recording the counter contents, accuracy was retained by splitting the count and using two analog channels per counter input. The 715 output is read out serially by single digits. The digital-to-analog converters

required were made to select any group of three digits for conversion to analog signal. The digital voltmeter input was for ±10 v full scale. For example, a counter content of 0023816 would be read by the logger as 2.38X v and 8.16X v, where X indicates the particular digit which is uncertain and outside the resolution of the counter. Any group of three consecutive digits may be read to either digital-to-analog converter so that the most significant digits may always be retained. Generally, the middle of five digits being recorded from the counter are overlapped by the two converters because of their ±(1/2) Least Significant Bit (LSB) accuracy. A block diagram of the CRC module is shown in Fig. 13. The CRC module provided the basic timing and control functions for the entire system.

In addition to the two counter channels, beam current and chamber pressure were recorded. Timing circuits initiated the recording of all four channels and manual inputs every 10 sec. The data logger punches paper tape which is used for access to an SDS 920 computer. A description of data reduction using the above parameters is discussed in a following section.

2.5 TEMPERATURE MEASUREMENTS

Whereas the wall temperature of the heated chamber was determined by thermocouples, the rotational temperature of N_2 was measured using the $N_2^+(1-)(0,0)$ band as just described. The rotational structure of the R-branch was resolved using 30-μm slit widths.

In the $\Delta v = -2$ sequence study, rotational lines were recorded in a continuous manner on a strip chart recorder, enabling peak values to be easily read. Using the method and tables of Ref. 9, the authors determined a rotational temperature from these peak values. At temperatures greater than 300°K, significant P-branch overlapping onto the R-branch begins, resulting in the lower rotational quantum number lines of the R-branch's exhibiting excessively large intensity values. No overlapped rotational line was used for the rotational temperature measurement.

In the $\Delta v = -3$ sequence study, eight digital data points typically formed the main envelope of each rotational line. Peak values were obtained from the intersection of the linear slopes forming each side of the line, and the above method was used to obtain the rotational temperature.

Figure 14 compares the measured rotational temperatures with the chamber heater thermocouple temperatures in the $\Delta v = -2$ and $\Delta v = -3$ sequence studies, and the results compare favorably. The (0,0) band scans at two temperatures of the $\Delta v = -3$ study are presented in Figs. 15 and 16.

SECTION III
EXPERIMENTAL RESULTS

The data acquisition method used for the $\Delta v = -2$ sequence allowed only total count summations to be made in the wavelength interval of interest. A poorly resolved spectrum, obtained using a slit width of 200 μm and a slit height of 5 mm, could have resulted if the successive differences in accumulated counts had been plotted versus wavelength, but these differences were used only to detect the start and end of the summation intervals. Background counts were subtracted from each count summation interval. The preliminary band intensity ratios were then calculated and corrected by the wavelength dependent spectral sensitivity factors. These ratios omit the influences of temperature-dependent rotational structure overlap onto succeeding bands and of other radiation appearing in the wavelength intervals. Total count estimates of two interfering nitrogen ion lines and a nitrogen molecular band were made from data plots of the accumulated counts. (The ion lines at 4630.54 and 4530.40 Å are in the R-branches of the (1,3) and (3,5) bands, respectively. The $N_2(2+)$ (1,6) band is in the (2,4) R-branch.) The preceding band ratios were then reduced by the counts fraction caused by each interfering ion or band intensity value. Three scans of the $\Delta v = -2$ sequence made during the higher resolution $\Delta v = -3$ sequence study revealed the presence of the 4601.48-Å nitrogen ion line. Although this line is only 1.7 Å from the (2,4) P-branch head, an estimate of its intensity was made and the (2,4)/(0,2) band intensity ratio subsequently corrected. Finally, the overlap calculations were performed to recover the experimental band intensity ratios.

The $\Delta v = -3$ sequence data, obtained using a slit width of 400 μm and slit height of 6 mm, were handled by SDS 920 and 9300 computer systems. Each count rate accumulated over a 10-sec interval was divided by the beam current, chamber pressure, and count interval time. Computer plots of these counts per second, per milliampere, and per millitorr allowed background intensity, the locations of interfering radiation, and summation intervals to be determined. Nitrogen ion lines at 5045.10, 5025.67, and 5016.39 Å in the (2,5) R-branch and the 4935.03-Å atom

line in the (4, 7) R-branch were principal contaminants. The (3, 6) band was completely buried in ion lines. In the second computer program, a wavelength was determined for each data point for which interpolated spectral sensitivity factors and backgrounds were calculated. For each point, the background was then subtracted and the resulting count rate divided by the spectral sensitivity factor. The relative photon rate was then obtained by dividing these count rates by the largest in the scan, and computer plots of relative photon rate versus wavelength were made. The resolved (0, 0) band and three $\Delta v = -2$ sequence data were handled similarly. The computer also summed the relative photon rate data over previously specified intervals, i.e., the (0, 3), (1, 4), (2, 5) and (4, 7) bands and some of the contaminants. Band intensity ratios were calculated from these summations and then corrected for overlap. Ratios were also calculated from the P-branch peaks, considering the neighboring band's R-branch overlap contribution.

Plots of the $\Delta v = -2$ sequence taken in the $\Delta v = -3$ sequence study are shown for two different temperatures in Figs. 17 and 18. These have been corrected for background, spectral sensitivity, and current and pressure fluctuations.

The two scans at 650°K provided information on the 4601.48-Å NII line contribution to the (2, 4) band relative photon rate. This wavelength region of one of the scans is shown in Fig. 19. Knowing the wavelength difference between the ion line and the P-branch peak and the ion line half-width, the authors obtained separated profiles. The result of this analysis was included in the $\Delta v = -2$ sequence study, and the fractional contributions were assumed to be constant for all temperatures.

A good background measurement existed just ahead of the (0, 2) bandhead, where no known radiation would appear. Because of band overlaps, another true background would not exist until the R-branch tail of the weak (3, 5) band was reached, where, at 300°K, the background appeared to be the same. At this point the background increased with temperature relative to the region near the (0, 2) bandhead, as would be expected. Therefore, each background was assumed equal to that near the (0, 2) bandhead and constant over the entire $\Delta v = -2$ sequence.

The experimental ratios were lastly modified by overlap corrections. To extract a total band intensity from a measured one, one must consider contributions from the R-branch tail of the preceding band and the loss of the R-branch tail into the following band. Let M^{ij} equal the R-branch

upper rotational quantum number at which the measurement for the total intensity S(ij) for the (i, j) band was cut off. For $M > M^{ij}$, the experimental intensity $S(ij)_{exp}$ was zero. Let the fractional intensity of the (i, j) band for $M > M^{ij}$ be α^{ij}. Then $\alpha^{ij} = S(ij,\ M > M^{ij})/S(ij)$. Considering the overlap case for each band, the following equations are derivable:

$$S(02) = S(02)_{Exp}/(1 - \alpha^{02})$$

$$S(ij)_{Exp}/S(02) = [S(ij)/S(02)]_{Exp}(1 - \alpha^{02})$$

$$S(13)/S(02) = \{[S(13)/S(02)]_{Exp} - \alpha^{02}\}/(1 - \alpha^{13})$$

$$S(24)/S(02) = \{[S(24)/S(02)]_{Exp} - \alpha^{13}[S(13)/S(02)]\}/(1 - \alpha^{24})$$

$$S(35)/S(02) = \{[S(35)/S(02)]_{Exp} - \alpha^{24}[S(24)/S(02)]\}/(1 - \alpha^{35})$$

The values of α^{ij} were obtained using a computer calculation of the theoretical relative intensity of each rotational line of each of the bands of interest of the $N_2^+(1-)$ system. Dipole rotational excitations were assumed, as stated previously, and, in addition to the obvious molecular parameters required, the dispersion and slit widths of the spectrometer are used as input data. The computer calculation has plotting provisions, and Fig. 20 presents a sample of the plotted output. Using the calculated R- and P-branch line intensities, the values of a^{ij} for each vibrational level were obtained. It was found that a^{ij} differed by less than 2 percent for all values of i and j for a given M^{ij}, and, consequently, the curve of Fig. 21 showing the variation of a^{ij} with M^{ij} is approximately valid for all values of i and j of this study. The values of M^{02}, M^{13}, M^{24}, and M^{35} are 26, 24, 22, and 20, respectively.

Table IV summarizes the results. Each fractional contribution by the 4574.3-Å $N_2(2+)$ (1, 6) band and 4530.40-Å NII line shown is the average of either three or four measurements. Since the 4630.54-Å NII line fractional contributions at all temperatures agreed well, a constant value was assumed. The two peak values reported for the (4, 6)/(0, 2) band ratio were estimates from the scans made in the $\Delta v = -3$ sequence study. Corrected plots of the $\Delta v = -3$ sequence at three temperatures are shown in Figs. 22 through 24.

Background determinations proved to be a difficult problem in the $\Delta v = -3$ sequence study. Band overlaps and contaminant radiation occupied wavelengths where molecular radiation would not ordinarily appreciably occur, and the signal-to-background ratio was very low for the weak bands. Figures 25 through 27 show the lowest count rate points. Surprisingly, the backgrounds just ahead of the (0, 3) bandhead were very inconsistent from run to run. Also, the 300°K backgrounds at 5240 Å were lower than those at 4940 Å, whereas the reverse was true for higher temperatures. The final assumed backgrounds are shown as solid lines on the figures.

The overlap equations and figures developed for the $\Delta v = -2$ sequence are applicable to the $\Delta v = -3$ sequence, provided the index j is replaced by (j+1). Much lower M^{ij} numbers were used since the band summations were cut off upon encountering contaminant radiation, whereas in the $\Delta v = -2$ sequence study the contaminants were initially included in the summation process. The M^{ij} numbers used for the (0, 3), (1, 4), (2, 5), (3, 6), and (4, 7) bands were 26, 25, 13, 21, and 9, respectively. Even though the (3, 6) band could not be measured, α^{36} and S(36)/S(03) were needed for the (4, 7) overlap calculation. For all temperatures the S(36)/S(03) ratios were assumed to be halfway between the S(25)/S(03) and S(47)/S(03) ratios. The final results are presented in Table V. Included are the ratios determined from P-branch peaks.

SECTION IV
DISCUSSION AND CONCLUSIONS

The experimental results at 300°K shown in Tables IV and V were used to obtain experimental values of $\sigma(vv'')/\sigma(00)$, the optical electron excitation cross section. For this purpose the predicted value of $\sigma(02)/\sigma(00)$ was employed for the normalization process. It should be noted that one measurement of the $\sigma(02)/\sigma(00)$ ratio was performed and that agreement with the predicted value listed in Table I was obtained. The values of $\sigma(vv'')/\sigma(00)$ thus obtained are listed in Table I. During the course of this investigation it was reported by Pendleton and O'Neil (Ref. 10) that the experimental values of $\sigma(vv'')/\sigma(00)$ as reported in Ref. 7 as well as their own data at room temperature exhibited an anomalous excess which appeared to be dependent only on v. In a similar manner the present data were analyzed, and an enhancement ratio, $\Gamma(vv'')$, was calculated for each $\sigma(vv'')/\sigma(00)$ experimentally measured, where

$$\Gamma(vv'') = [\sigma(vv'')/\sigma(00)]_{Exp} / [\sigma(vv'')/\sigma(00)]_{Theo.} \quad (8)$$

Using the values $\Gamma(vv'')$ and the experimental uncertainty $\Delta\Gamma(vv'')$, the authors calculated a weighted mean and standard deviation for each value v for each temperature if data of more than one sequence existed at that temperature. The results yield $\Gamma(v)$ and the one-sigma uncertainty $\Delta\Gamma(v)$. The results are shown in Fig. 28. At 660 and 880°K the values of $\Gamma(4)$ using the values obtained from the peaks of the (4, 6) band are also shown. These values were not averaged with the integrated sums of the (4, 7) band but are shown for comparison. Figure 28 shows the excellent agreement of the results with the predicted values for v = 1 over the entire temperature range. Additionally, the trend of decreasing $\Gamma(v)$ as temperature increases above 660°K for all values of v is evident. However, $\Gamma(4)$ does exhibit a maximum at 660°K for the (4, 6) peak value as well as for the (4, 7) integrated sum.

Values of $\sigma(v)/\sigma(0)$ were calculated using the measurements of $\Gamma(v)$ at 300°K, and both sets of parameters are listed in Table VI. Also shown in Table VI are the experimental values of $\sigma(v)/\sigma(0)$ obtained by Stanton and St. John (Ref. 7), and it is seen that the results differ at most by approximately 20 percent.

The possible causes of the observed enhancement will now be considered:

1. Inaccurate emission band strengths:
   This cause is dismissed since enhancement is observed to be temperature dependent as well as present for two different sequences for the same vibrational level.

2. Requirement of excitation band strengths in lieu of Franck-Condon factors:
   To investigate this possibility it was assumed that $\tilde{p}(vv')$ varied linearly with $\bar{r}(vv')$; i. e.,

$$\tilde{p}(vv') = \tilde{q}(vv')[1 + b\,\bar{r}(vv')] \quad (9)$$

   Values of $S(v_1v_1'')/S(v_2v_2'')$ were calculated for several values of b within the range $0 \leq b \leq 5$. Figure 29 shows the resulting enhancement ratio as a function of b for T = 300°K. From Fig. 29 it is obvious that a nonzero value of b is not an explanation of the experimental results.

First, even for values of b as large as 5, which is considered to be excessively high, the enhancement of v = 4, $\Gamma(4)$ is approximately 2.5, nearly two orders of magnitude smaller than the observed effect, and a similar conclusion is reached for $\Gamma(3)$. Secondly, one cannot argue convincingly for b to exceed 1.00, since any larger value would destroy the excellent experimental agreement with predicted values for v = 1. An almost identical conclusion was reached by Williams, Hornkohl and Lewis (Ref. 3) on the basis of T_v measurements of N_2 in a hypersonic flow field.

3. Nonequilibrium ground state vibrational distribution: Since enhancement was observed at 300°K and also at higher temperatures for which the gas source produced Boltzmann distributions in the vibrational levels of $N_2 X\ ^1\Sigma_g^+$, it must be that nonequilibrium distributions would result only as a result of electron collisions. For this case one would expect to observe nonlinearities of $S(v_1 v_2'')$ with beam current, but such was not the case.

4. Perturbation of the $N_2^+ B\ ^2\Sigma_u^+$ state: It is known that the levels v = 2, 3, and 4 of $N_2^+ B\ ^2\Sigma_u^+$ are perturbed by the $A\ ^2\Pi_u$ state. Consequently, the eigenfunctions of these levels are mixtures of the $N_2^+ B\ ^2\Sigma_u^+$ and $N_2^+ A\ ^2\Pi_u$ states, and the possibility exists that the Morse function excitation Franck-Condon factors are inaccurately calculated. If one increases the values of $\tilde{q}(2,0)$, $\tilde{q}(3,0)$, and $\tilde{q}(4,0)$ by the appropriate values of $\Gamma(v)$ at 300°K, the resulting theoretical values of the intensity ratios provide order of magnitude, or better, agreement with the experimental results. Additionally, it is noted that such changes in $\tilde{q}(v \geq 2, v')$ affect the orthonormality relations

$$\sum_{v'} \tilde{q}(v,v') = 1$$
$$\text{or}$$
$$\sum_{v} \tilde{q}(v,v') = 1$$

by less than approximately six parts per thousand in the worst case. Despite the approximate agreement between experimental and calculated values rendered by scaling the excitation parameters, it is difficult to accept this as the source of the enhancement since the Rydberg-Klein-Rees (RKR) excitation parameters, which are inherently more accurate than the Morse calculations, are in approximate agreement with the results of the Morse calculations.

5. Cascading and Auto-Ionization Effects:
To date, no radiative cascading has been reported as a population mechanism of the $N_2^+B\ ^2\Sigma_u^+$ state from valence shell N_2^+ states of electronic excitation. Neither do the recent measurements of El-Sherbini and Van Der Wiel (Ref. 11) of the oscillator strength of the $N_2^+B\ ^2\Sigma_u^+$ state exhibit any pronounced auto-ionization excitation processes. However, the companion paper (Ref. 12) of Ref. 11 does present data which may well be related to the enhancement observed in the present work. Reference 12 reports K-shell excitation of the $N_2X\ ^1\Sigma_g^+$ ground state $(\sigma_g 1s)^2(\sigma_u 1s)^2(\sigma_g 2s)^2(\sigma_u 2s)^2(\pi_u 2p)^4(\sigma_g 2p)^2$ by 10-keV electrons to the molecular configuration $(\sigma_g 1s)^2(\sigma_u 1s)^1(\sigma_g 2s)^2(\sigma_u 2s)^2(\pi_u 2p)^4(\sigma_g 2p)^2(\pi_g 2p)^1$ which is designated as N_2^{K*} in Ref. 12. Subsequent Auger electron decay of the N_2^{K*} state to the $N_2^+X\ ^2\Sigma_g^+$, $A\ ^2\Pi_u$ and $B\ ^2\Sigma_u^+$ states was observed. Additionally, the energy width of the $B\ ^2\Sigma_u^+$ population process is not sharp, and one expects population of a range of vibrational levels of the $B\ ^2\Sigma_u^+$ state. The inclusion of the Auger decay $N_2^{K*} \rightarrow B\ ^2\Sigma_u^+$ population mechanism requires replacement of $\sigma(v)$ by

$$\sigma(v) + \sigma(N_2^{K*}) \times \beta(N_2^{K*}, v)$$

where $\sigma(N_2^{K*})$ is the excitation cross section of the N_2^{K*} state from the electronic ground state and $\beta(N_2^{K*}, v)$ is the molecular branching factor for the Auger decay to level v of the $B^2\Sigma_u^+$ state. It is assumed that no other cascading processes exist. Furthermore, it is well known that for low atomic number species K-shell X-ray fluorescence yields are negligible, and therefore the branching factor for population of the $B^2\Sigma_u^+$ state is determined primarily by the magnitude of competing Auger decay channels of the N_2^{K*} state, none of which is known at present. However, the differential oscillator strength data of Ref. 12 support the hypothesis that Auger decay processes may be a significant population source for the $B^2\Sigma_u^+$ state so long as the appropriate molecular branching factors are not negligible. If this is the case, the results of the present work indicate a preferential population of the levels $B^2\Sigma_u^+(v \geq 2)$.

One may assume the apparent electron excitation cross section to be

$$[\sigma(v)/\sigma(0)]_{Exp} = \sigma(v)/\sigma(0) + \sigma'(v)/\sigma(0) \tag{10}$$

where $\sigma'(v) = \sigma(N_2^{K*})\ \beta(N_2^{K*} v)$, $v \geq 2$, and $\sigma(v)/\sigma(0)$ is the theoretical cross-section ratio representing direct $B^2\Sigma_u^+$ excitation. Figure 30 shows the temperature variation of the cross-section ratio $\sigma(v)/\sigma(0)$, v = 1, 2, 3, and 4. To determine the temperature variation of the ratios $\sigma'(v)/\sigma(0)$, $v \geq 2$, the experimental values of $\sigma(v)/\sigma(0)$ shown in Fig. 31 were used. For this purpose for v = 2 at 300 and 900°K the -2 and -3 sequence averaged data were used, and at 600 and 800°K the more accurate -2 sequence data were used. For v = 3, only -2 sequence data exist, and for v = 4, only -3 sequence data were obtained. Using Eq. (10) and the data of Figs. 30 and 31, the authors found the temperature variation of $\sigma'(v)/\sigma(0)$, and the results are shown in Fig. 32. The results of Fig. 32 clearly show the desirability of further measurements at temperatures exceeding those of the present work.

In summary, the relative optical and apparent electron excitation cross sections of the N_2^+ First Negative System have been measured over the temperature range from 300 to 900°K. Temperature-dependent enhancement was found for emission from the levels $B\,^2\Sigma_u^+$ (v = 2, 3, and 4). The most likely origin of the enhancement appears to be secondary excitation mechanisms, of which Auger electron decay following K-shell excitation is suggested as the most likely. It is suggested that further studies of the enhancement mechanism be conducted to extend the temperature range of the present work and that limited measurements of the electron energy dependence of the enhancement be performed.

REFERENCES

1. DeLeeuw, J. H. and Daves, W. E. R. "Measurement of Temperature and Density in the Upper Atmosphere Using an Electron Beam." Canad. J. Phys., 50 (1972), 1044-1052.
2. Justus, C. G. and Woodrum, Arthur. "Atmospheric Pressure, Density, Temperature and Wind Variations Between 50 and 200 KM." NASA CR-2062, May 1972.
3. Williams, W. D., Hornkohl, J. O., and Lewis, J. W. L. Electron Beam Probe for a Low Density Hypersonic Wind Tunnel." AEDC-TR-71-61 (AD727004), July 1971.
4. Wallace, L. V. and Nicholls, R. W. "The Interpretation of Intensity Distributions in the N_2 Second Positive and N_2^+ First Negative Band System." J. Atmos. Terrest. Phys., 24 (1962), 749.
5. Tyte, D. C. and Nicholls, R. W. "Identification Atlas of Molecular Spectra, 3: The $N_2^+ B\,^2\Sigma_u^+ - X\,^1\Sigma_g^+$ First Negative System of Nitrogen." The University of Western Ontario, London, Ontario, April 1965.
6. Bennett, R. G. and Dalby, F. W. "Experimental Determination of the Oscillator Strengths of the First Negative Bands of N_2^+." J. Chem. Phys., 31 (1959), 434-441.

7. Stanton, P. N. and St. John, R. M. "Electron Excitation of the First Positive Bands of N_2 and of the First Negative and Meinel Bands of N_2^+." J. Opt. Soc. Amer., 59 (1969), 252-260.

8. Schweiger, G., Wanders, K., and Becker, M. "Influence of Electron Beam-Blunt Body Interactions on Density Measurements in Transition Flow." Eighth International Symposium on Rarefied Gas Dynamics, Abstracts, AFOSR-TR-72-1276, July 1972.

9. Robben, F. and Talbot, L. "Some Measurements of Rotational Temperatures in a Low Density Wind Tunnel Using Electron Beam Fluorescence." AS-65-5 (AD466305), May 1965.

10. Pendleton, W. R. and O'Neil, R. "Departure of $N_2^+(B\ ^2\Sigma_u^+,\ v' = 2$ and 3) Vibrational Populations from Franck-Condon Predictions in the Case of Energetic e - $N_2(X\ ^1\Sigma_g^+,\ v = 0)$ Collisions." J. Chem. Phys., 56 (1972), 6260-6262.

11. El-Sherbini, Th. M. and Van Der Wiel, M. J. "Ionization of N_2 and CO by 10 keV Electrons as a Function of the Energy Loss, I: Valence Electrons." Physica, 59 (1972), 433-452.

12. El-Sherbini, Th. M. and Van Der Wiel, M. J. "Ionization of N_2 and CO by 10 keV Electrons as a Function of the Energy Loss, II: Inner-Shell Electrons." Physica, 59 (1972), 453-462.

APPENDIXES

I. ILLUSTRATIONS

II. TABLES

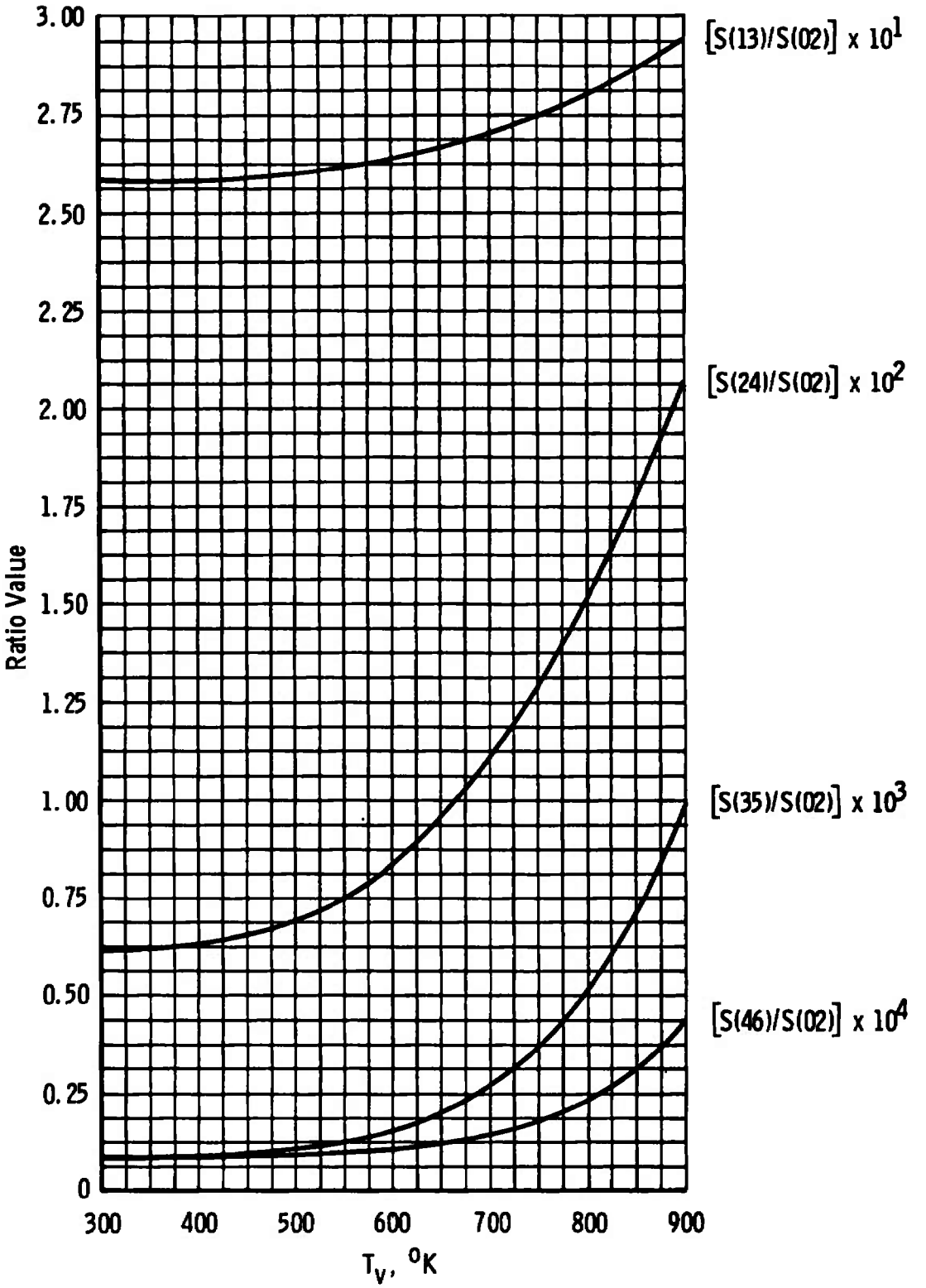

Fig. 1 N_2^+(1-) Δv = -2 Sequence Band Intensity Ratios versus Vibrational Temperature

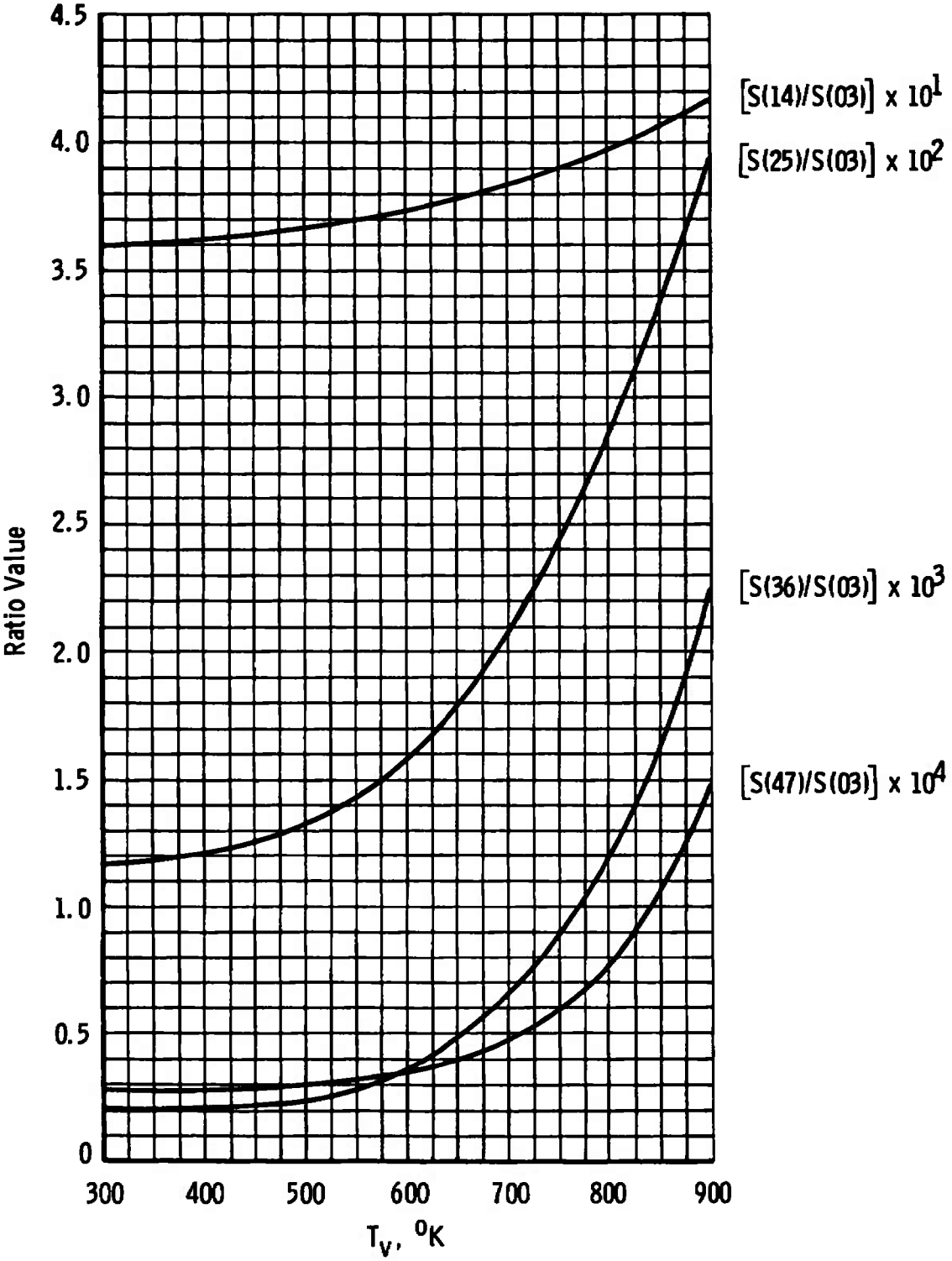

Fig. 2 N_2^+(1-) Δv = -3 Sequence Band Intensity Ratios versus Vibrational Temperature

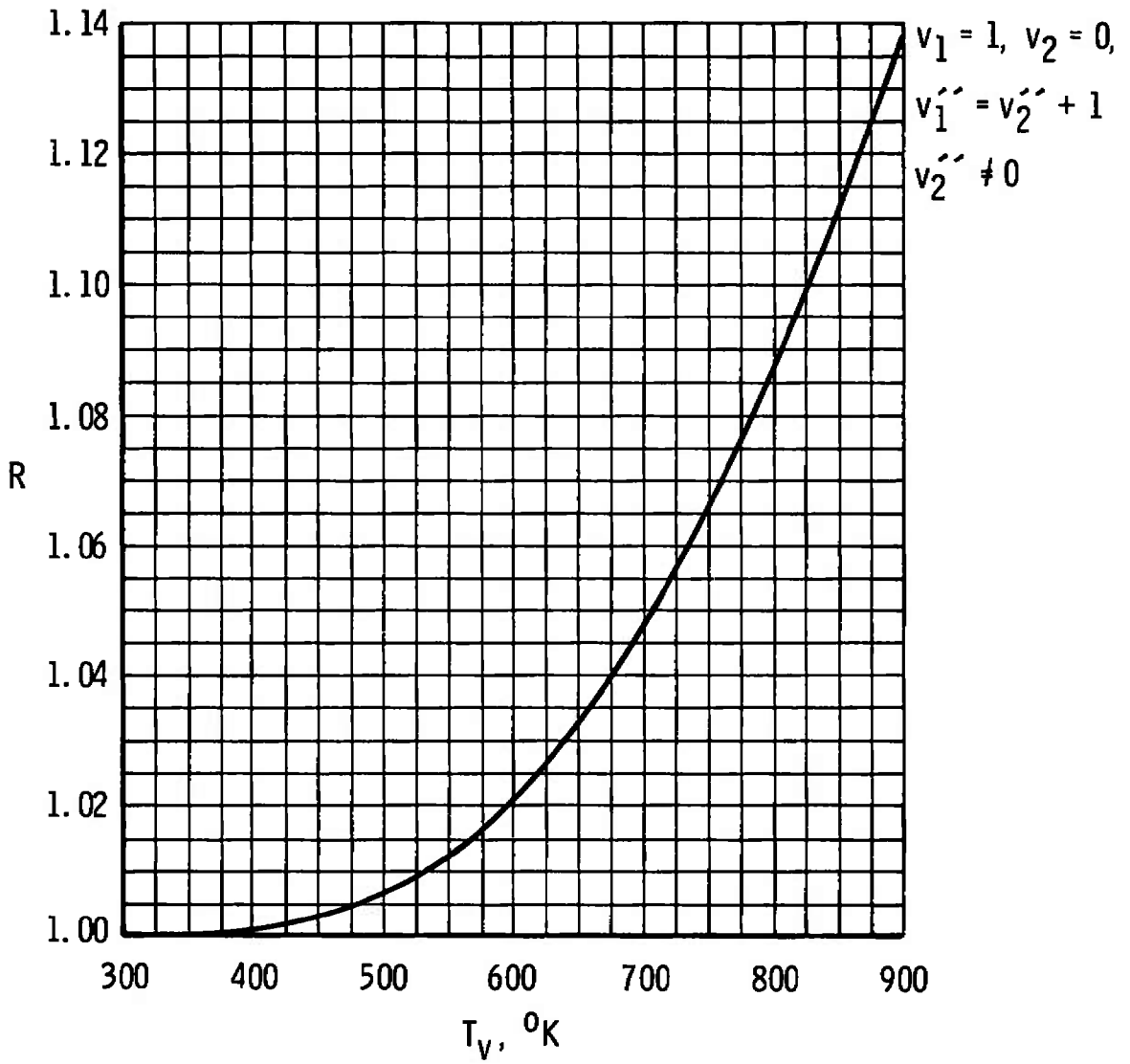

Fig. 3 Band Intensity Ratios Normalized to 300°K Value versus Vibrational Temperature

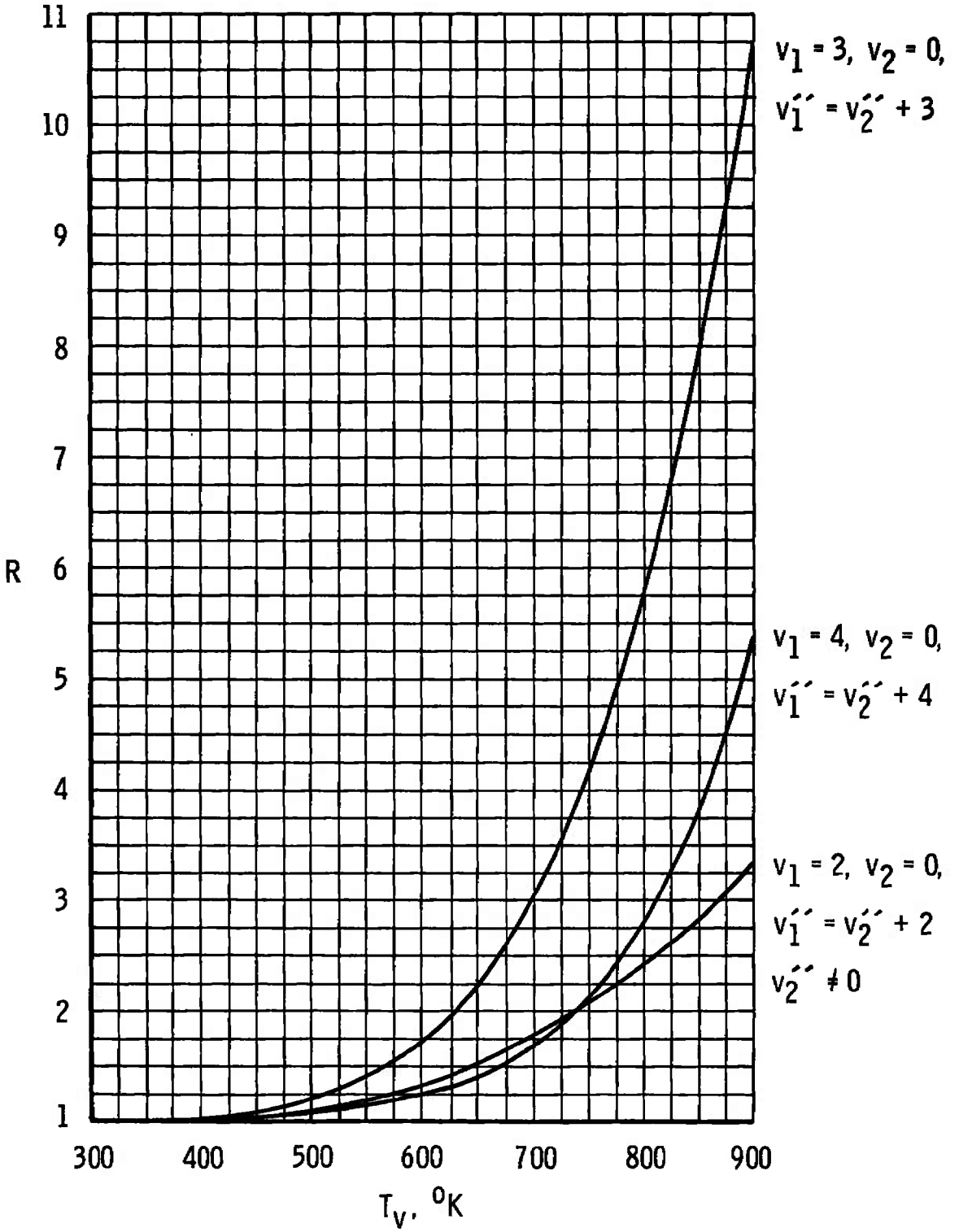

Fig. 4 Band Intensity Ratios Normalized to 300°K Value versus Vibrational Temperature

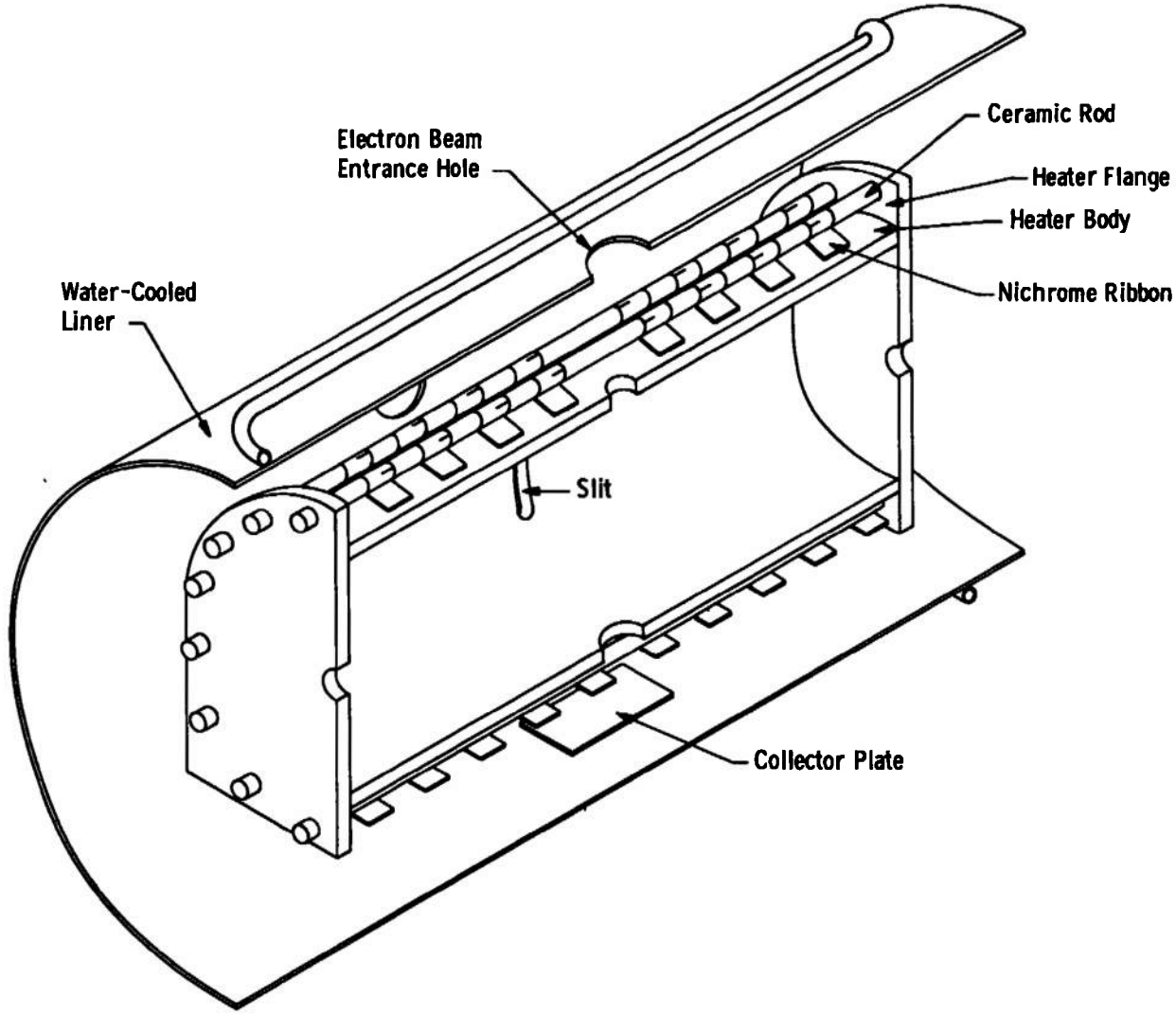

Fig. 5 Cutaway Schematic of Heater and Water-Cooled Liner

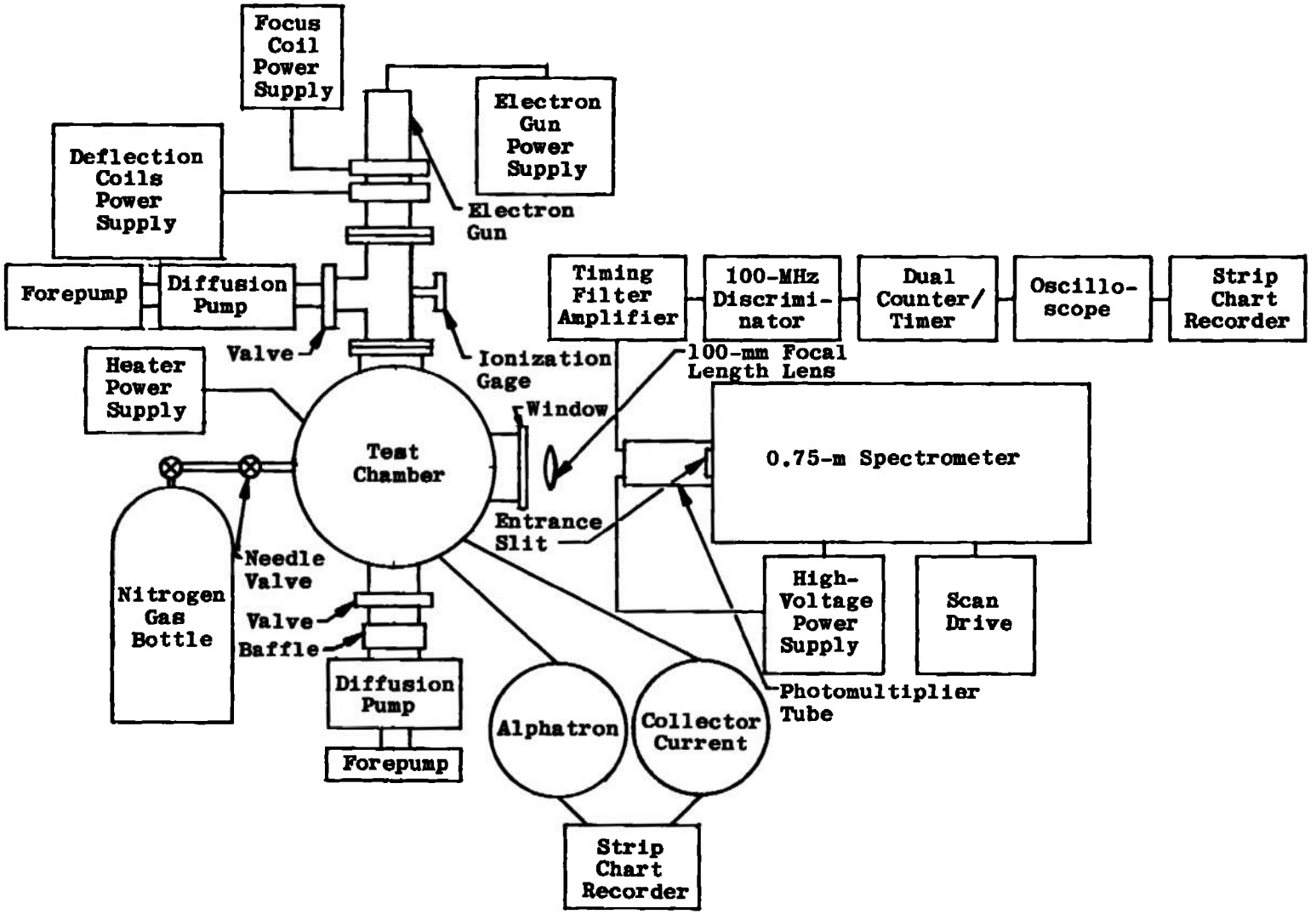

Fig. 6 $\Delta v = -2$ Sequence Study Block Diagram

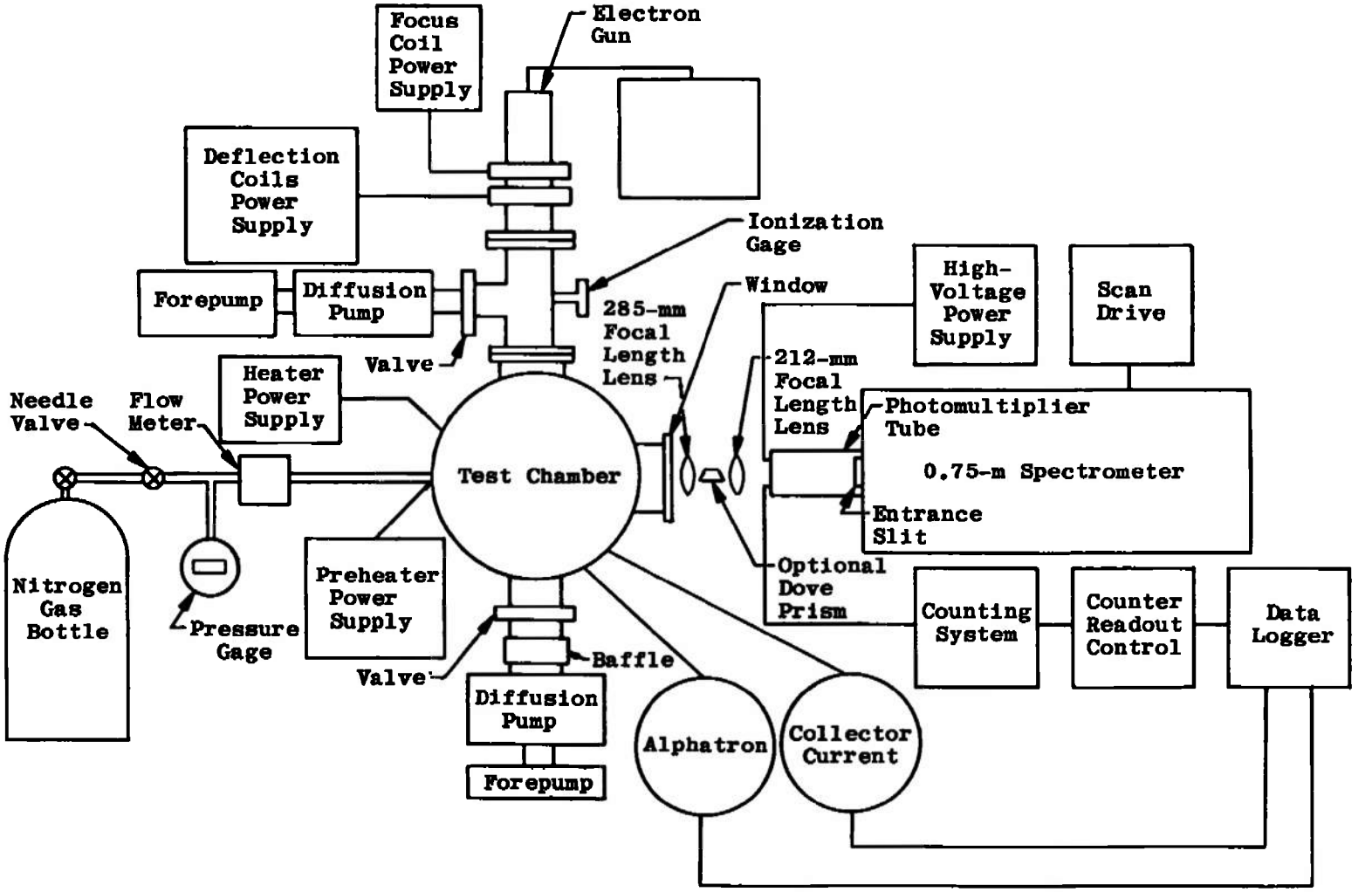

Fig. 7 Δv = -3 Sequence Study Block Diagram

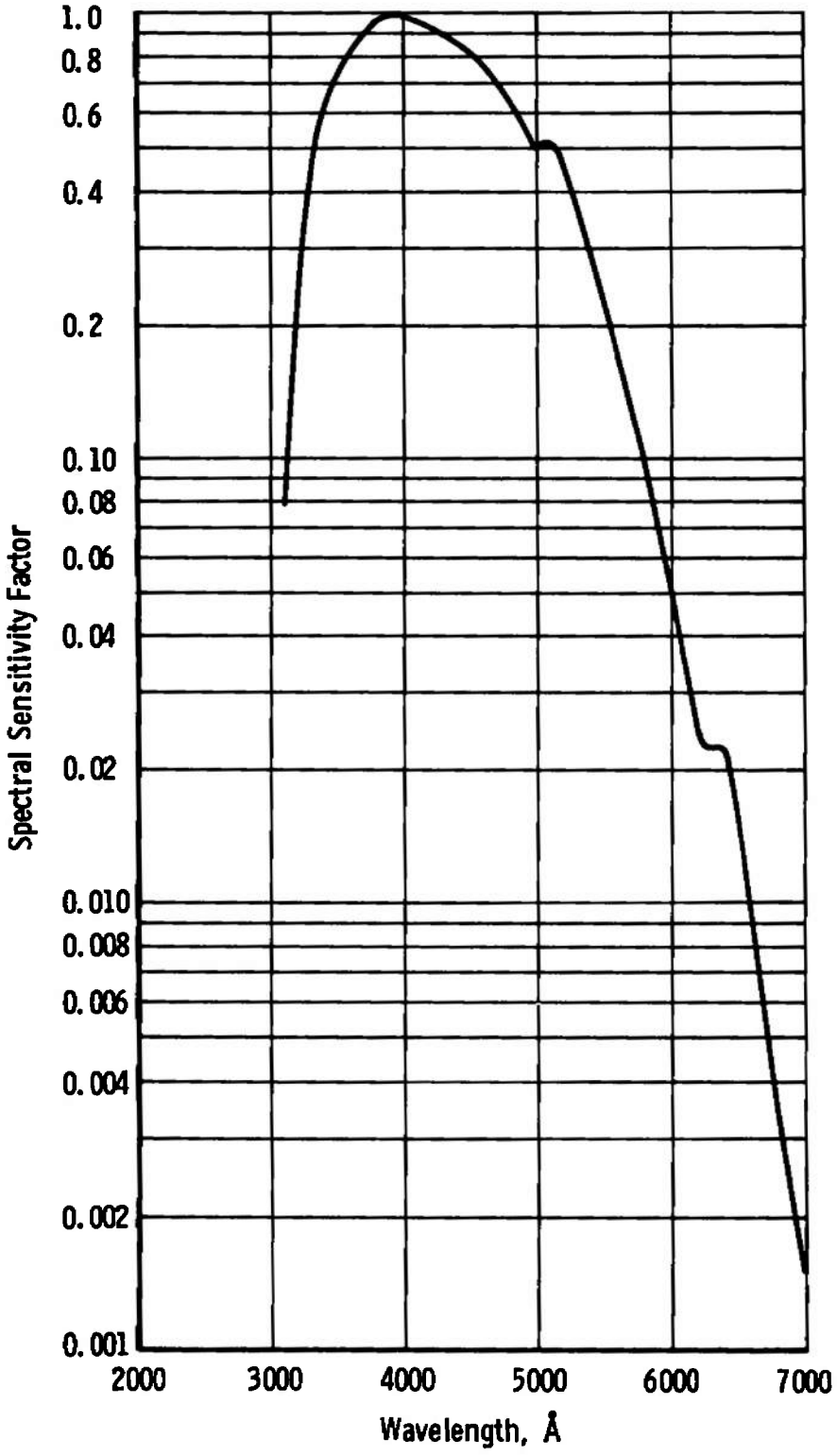

Fig. 8 Spectral Sensitivity Curve for $\Delta v = -2$ Sequence Study

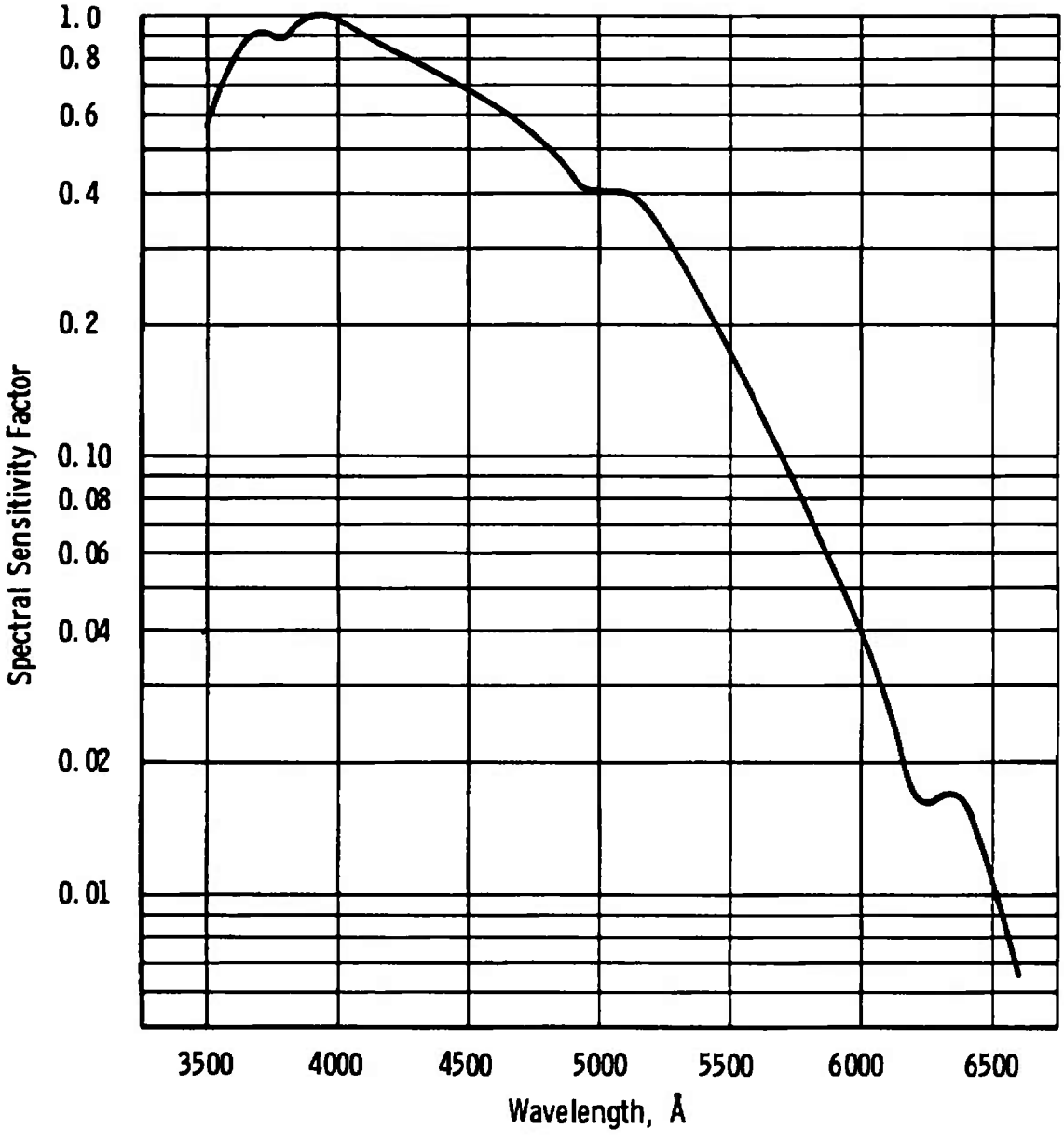

Fig. 9 Spectral Sensitivity Curve for $\Delta v = -3$ Sequence Study

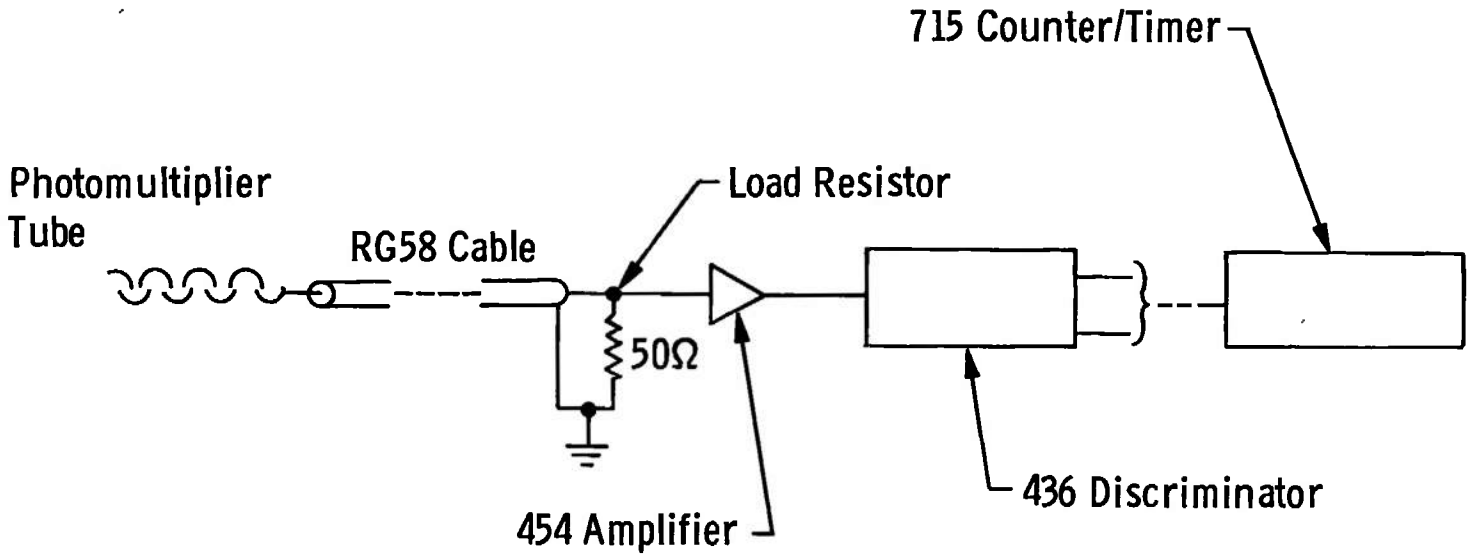

Fig. 10 Block Diagram of ORTEC Photon Counting System

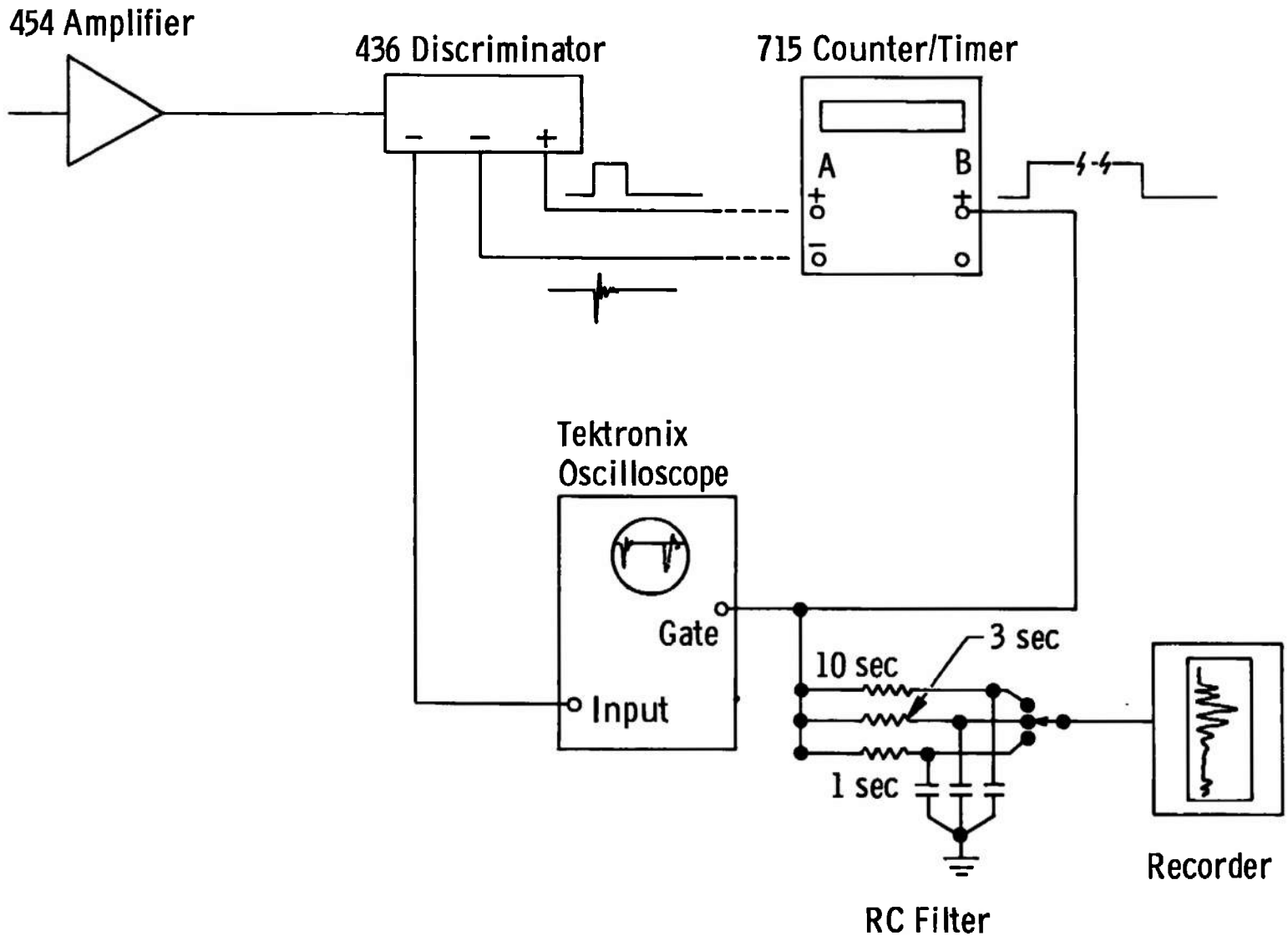

Fig. 11 Block Diagram of Analog System for Rotational Temperature Measurements

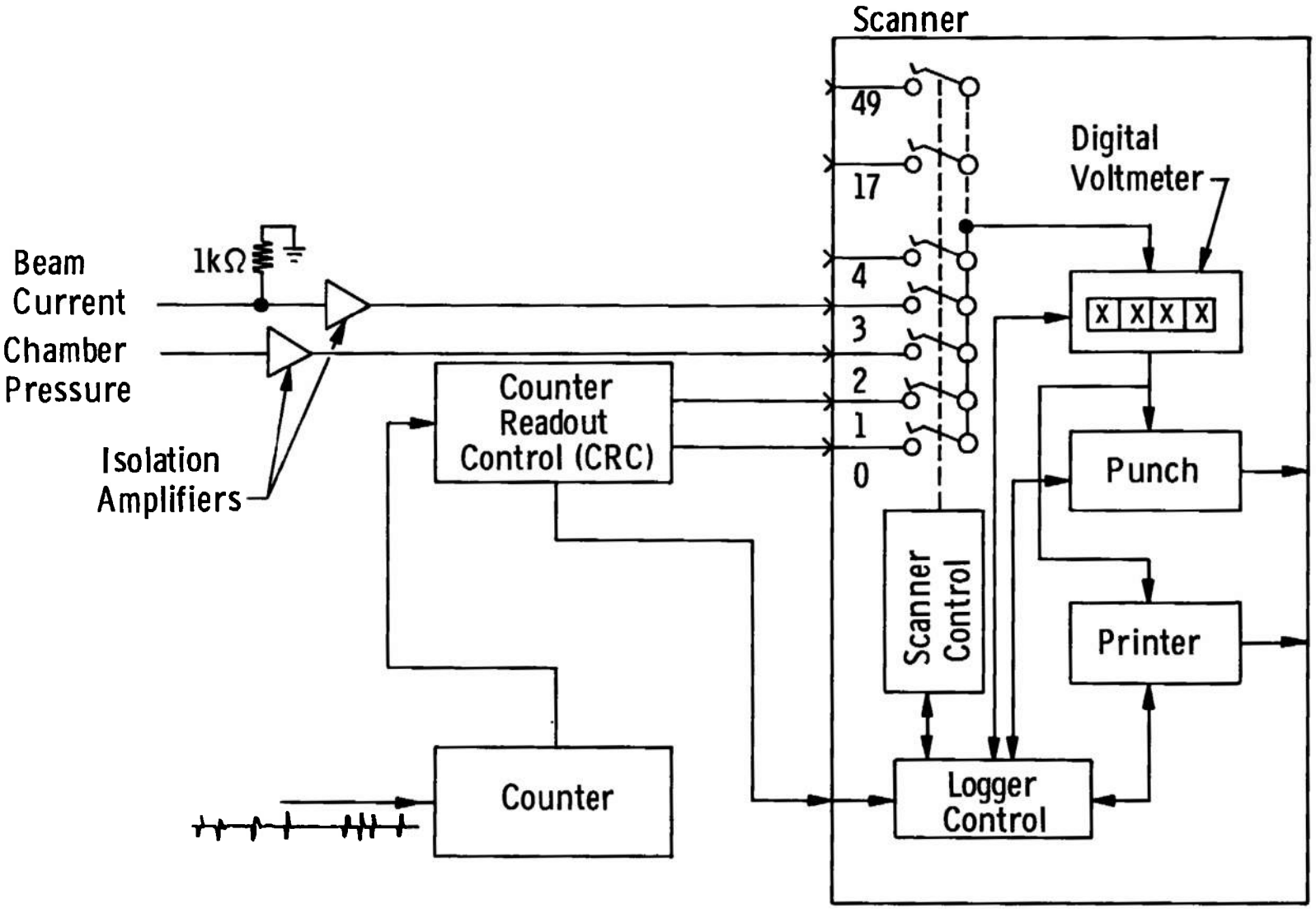

Fig. 12 Block Diagram of Data Logger System

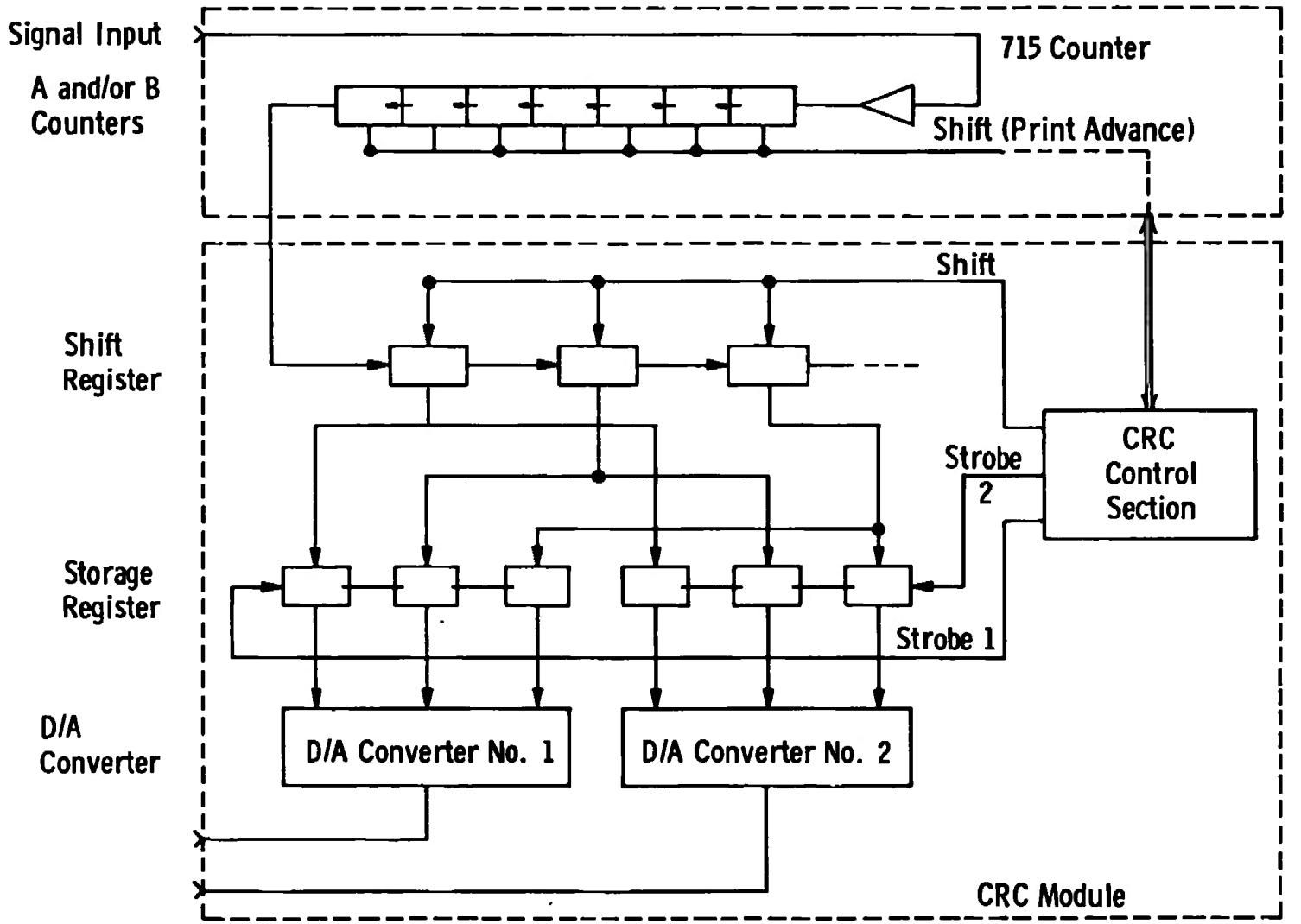

Fig. 13 Block Diagram of Counter Readout Control (CRC) Module

AEDC-TR-73-28

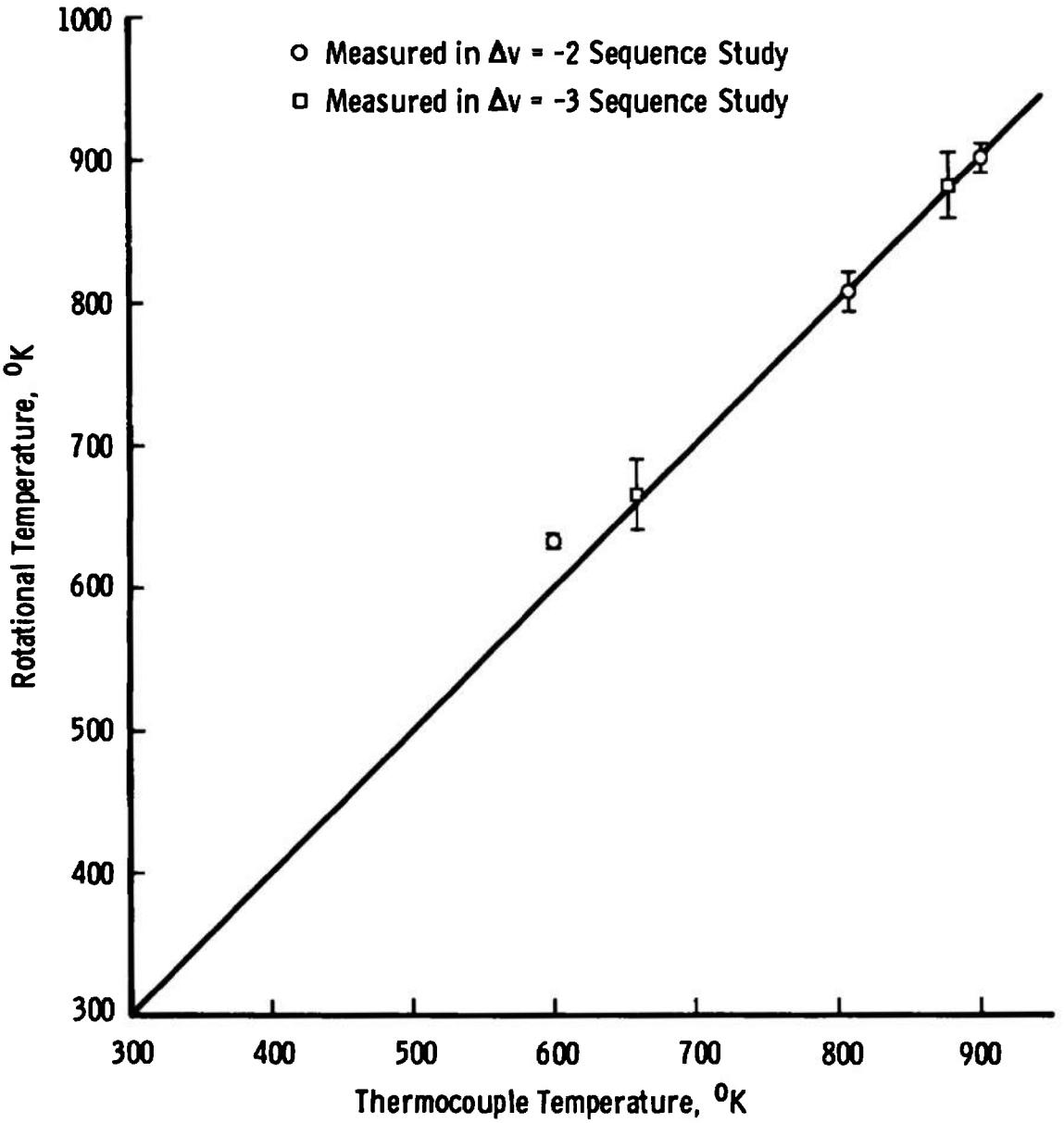

Fig. 14 Measured Rotational Temperature versus Thermocouple Temperature

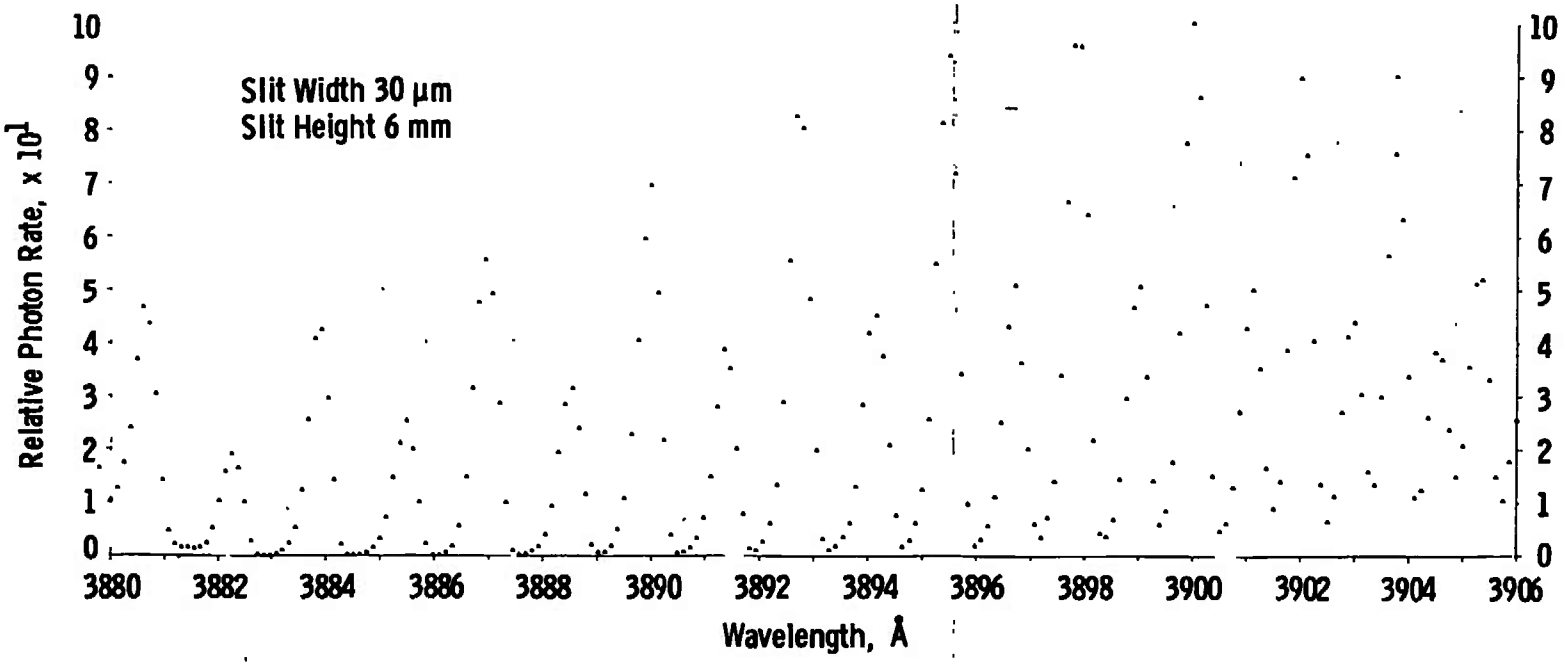

Fig. 15 Resolved N_2^+(1-) (0,0) Band at 660°K

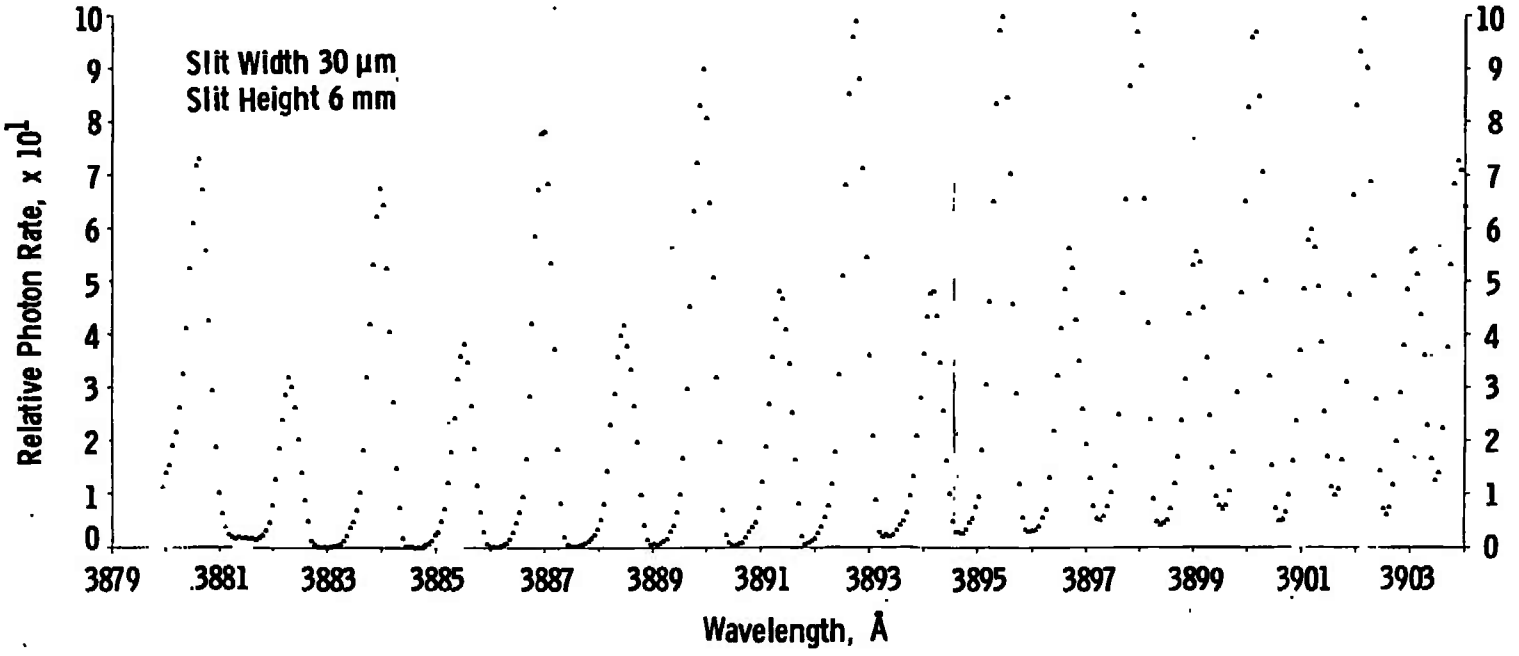

Fig. 16 Resolved N_2^+(1-) (0,0) Band at 880°K

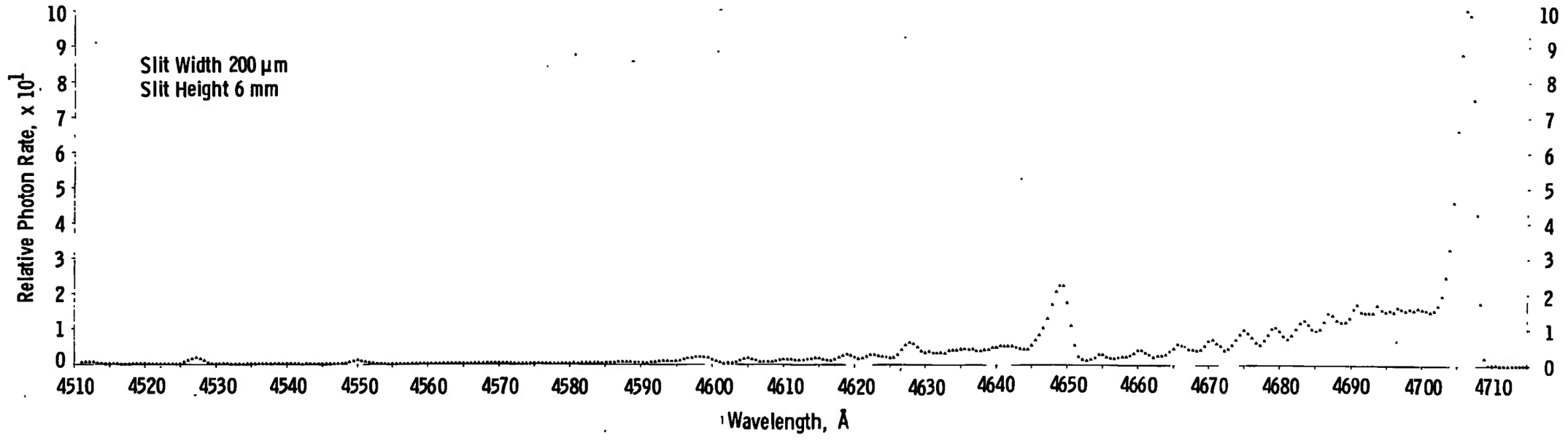

Fig. 17 $N_2^+(1-)$ $\Delta v = -2$ Sequence at 660°K

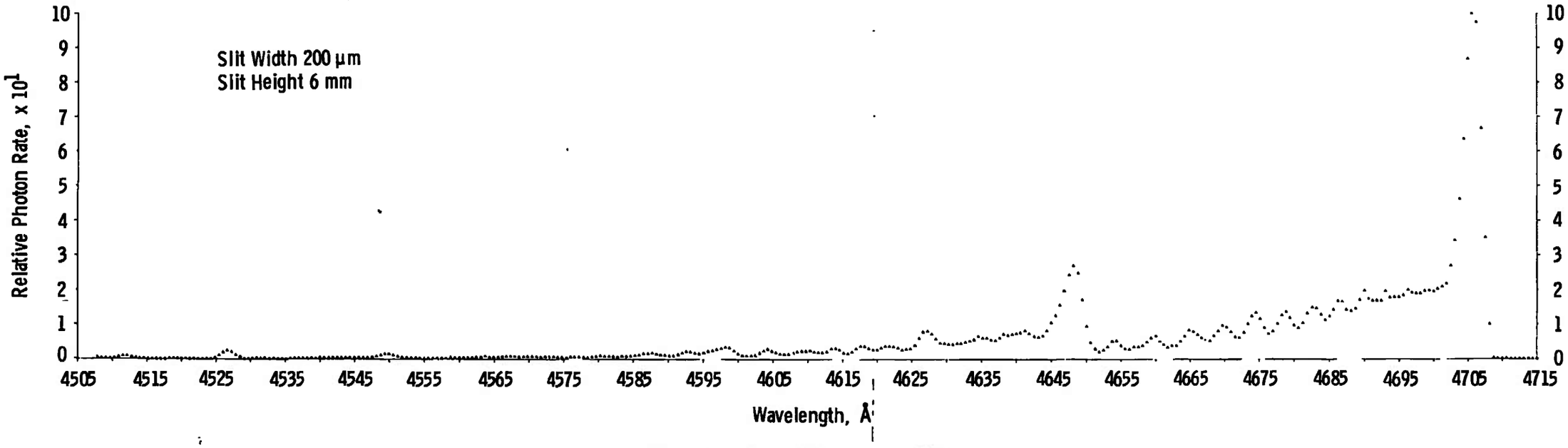

Fig. 18 $N_2^+(1-)$ $\Delta v = -2$ Sequence at 880°K

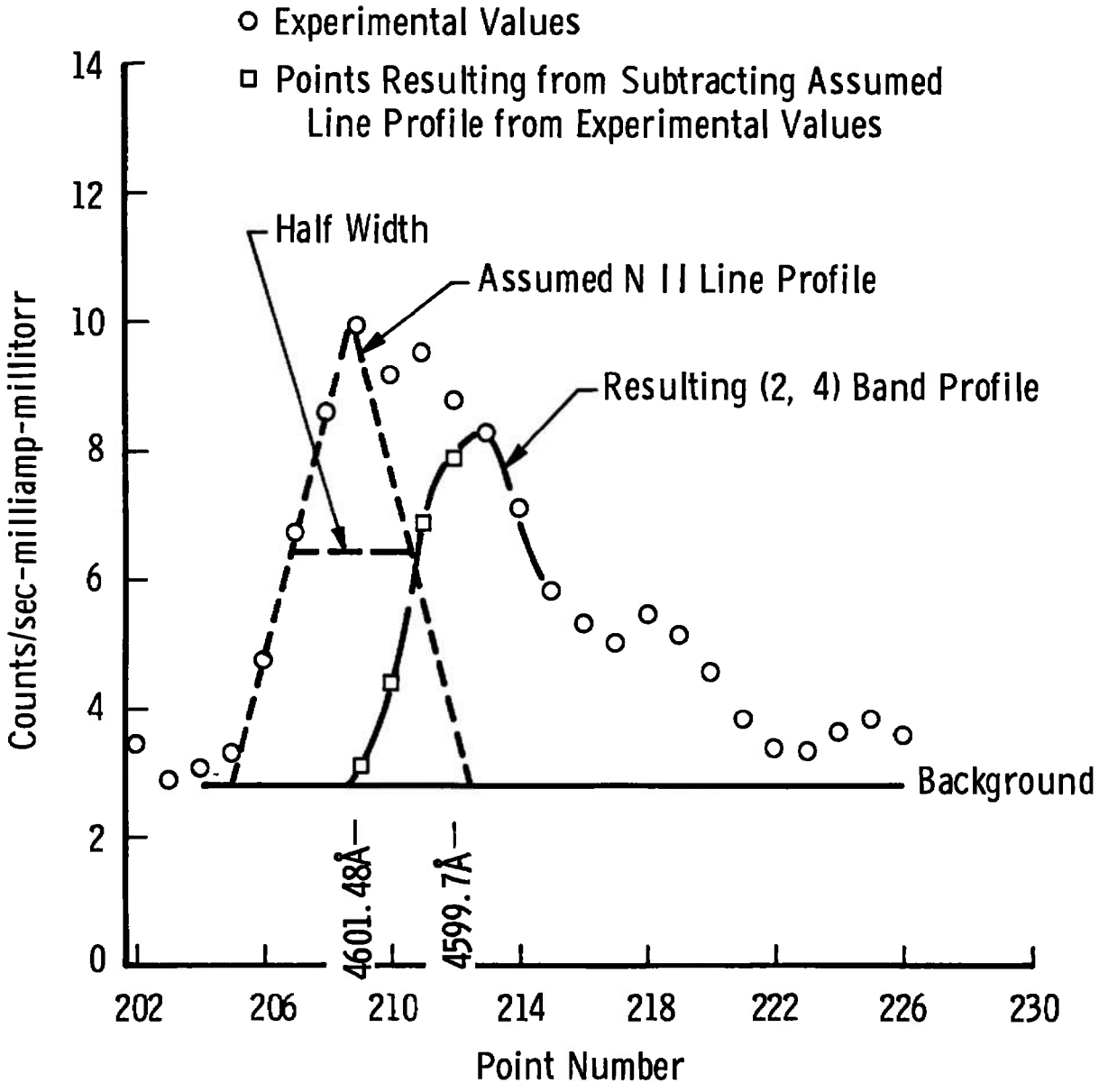

Fig. 19 Separation of 4601.48-Å NII Line and (2,4) Band

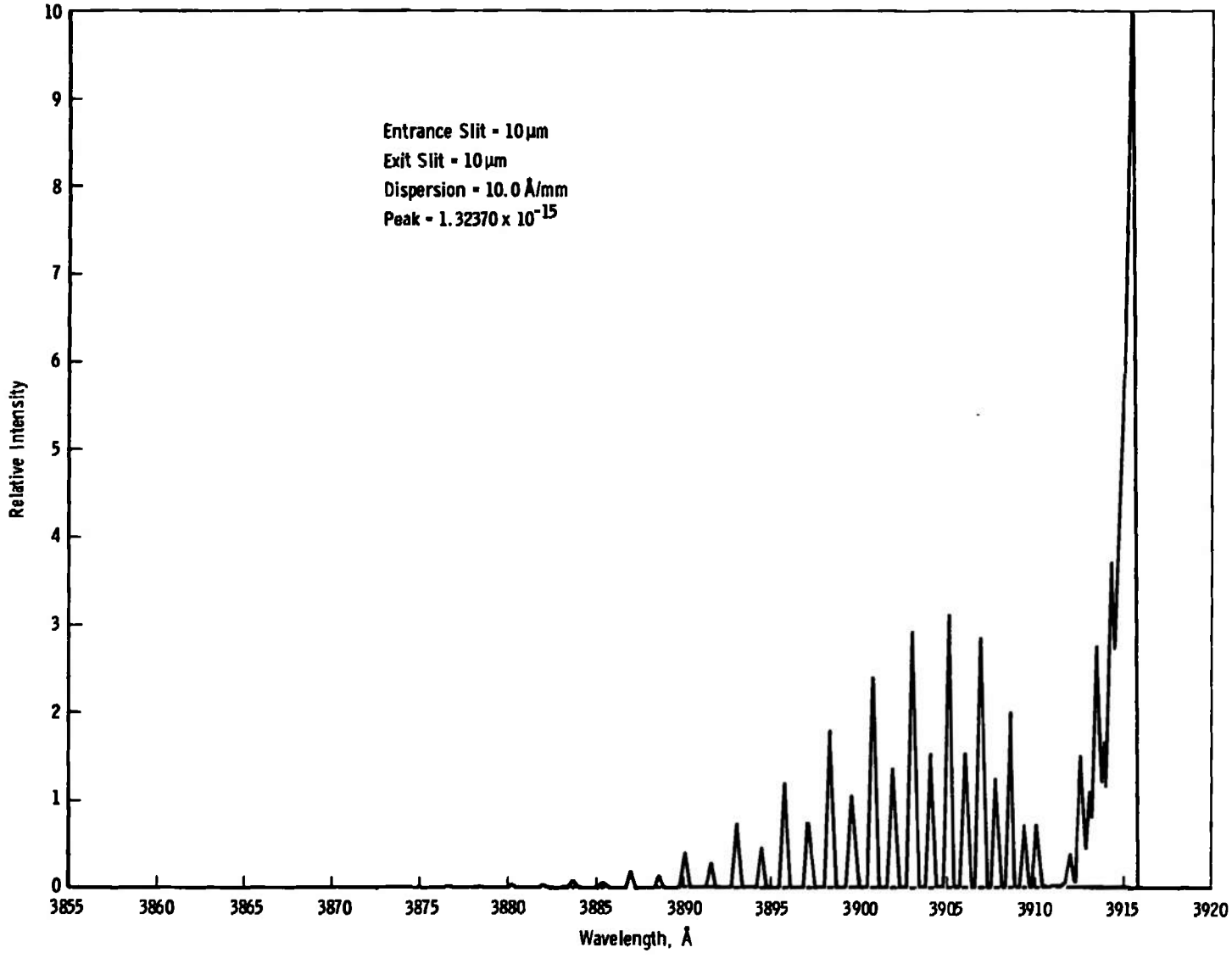

Fig. 20 Computer Plot of N_2^+ (1-)(0,0) Band at 300°K

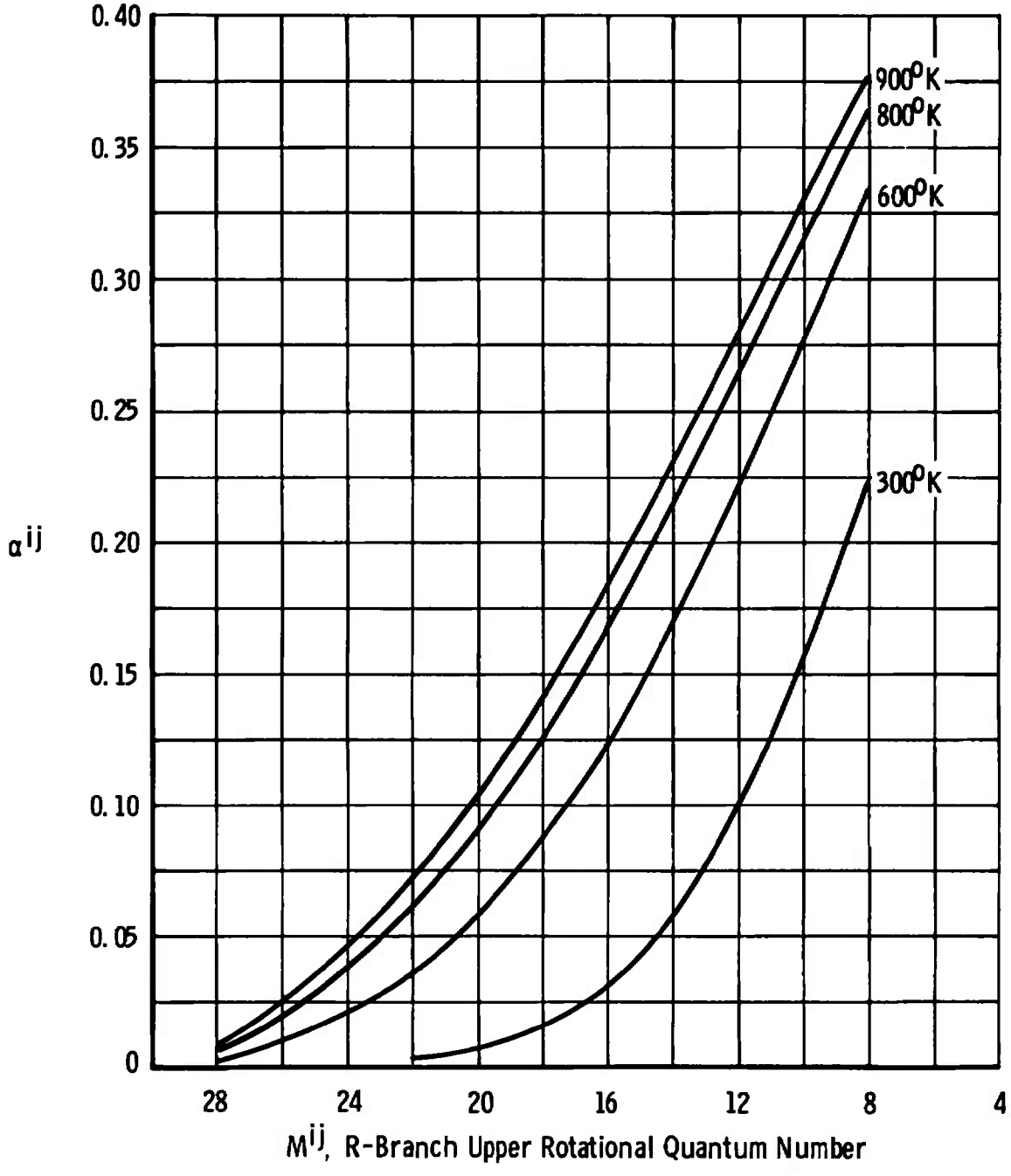

Fig. 21 Band Overlap Fraction α^{ij} versus R-Branch Quantum Number at Cutoff

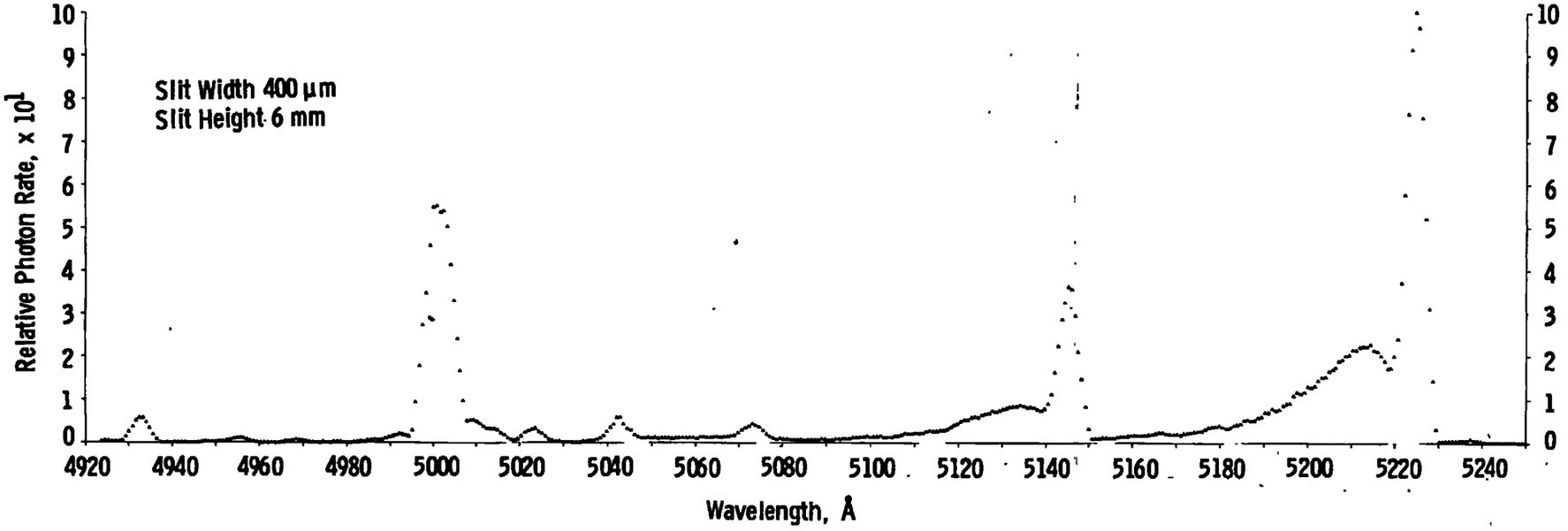

Fig. 22 N_2^+(1-) $\Delta v = -3$ Sequence at 300°K

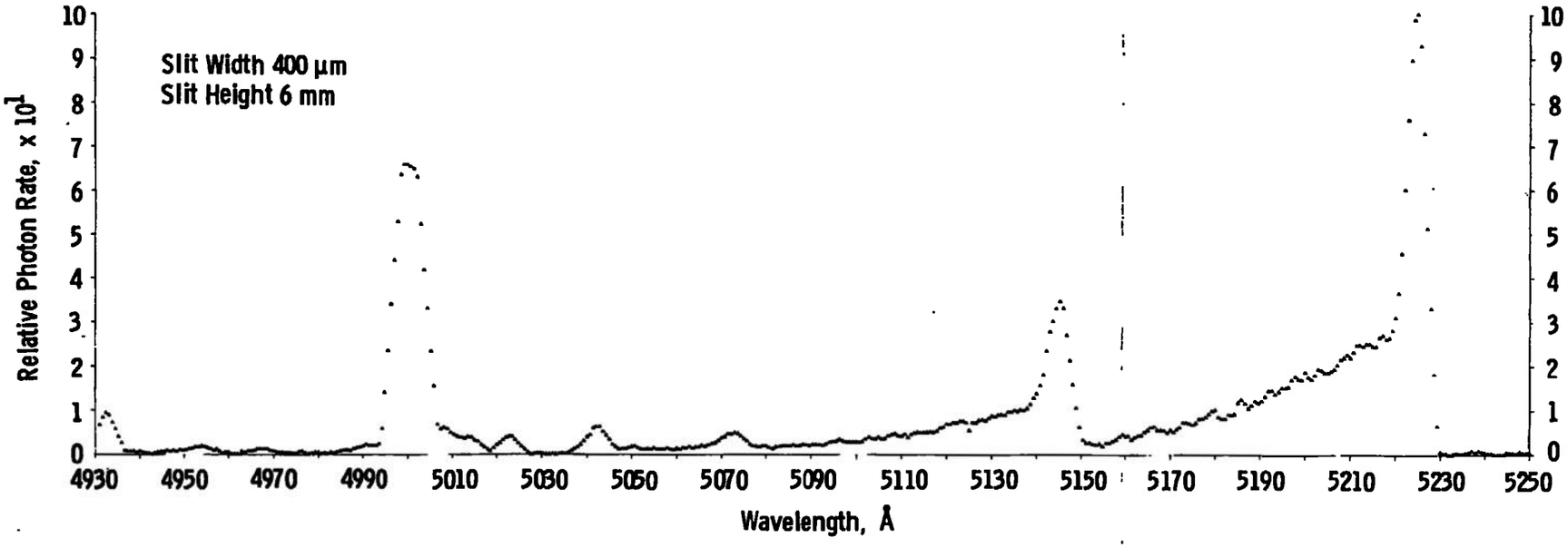

Fig. 23 N_2^+(1-) $\Delta v = -3$ Sequence at 660°K

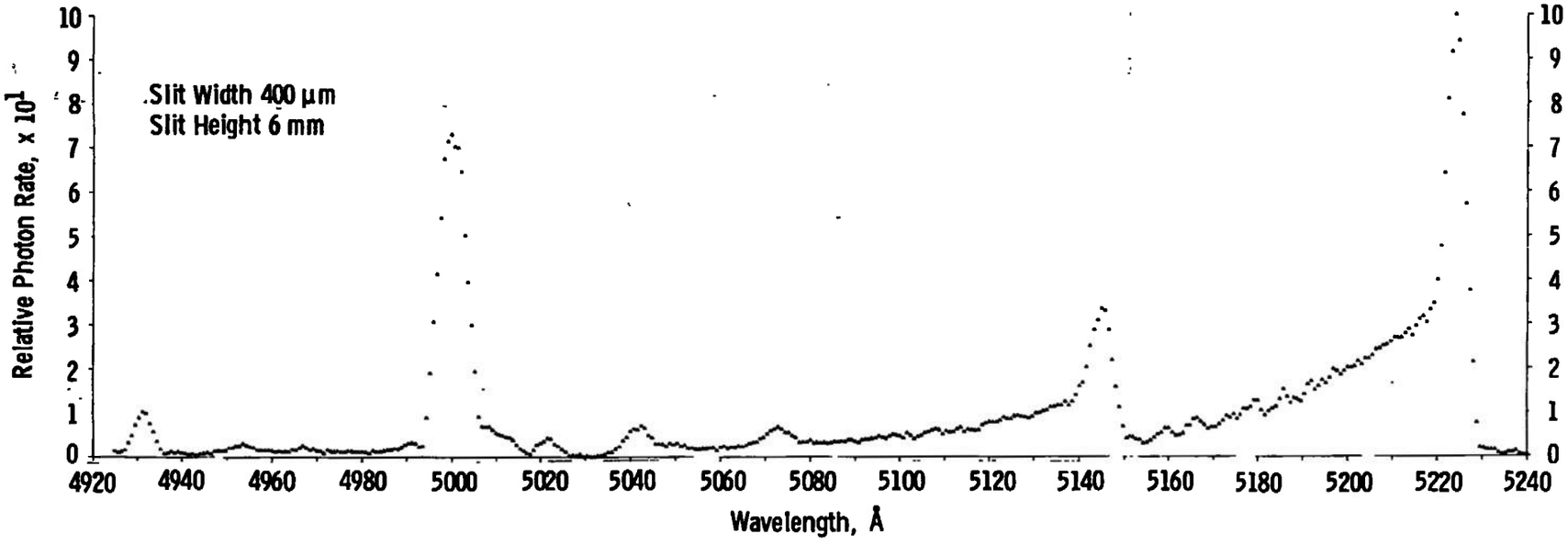

Fig. 24 $N_2^+(1-)$ $\Delta v = -3$ Sequence at 880°K

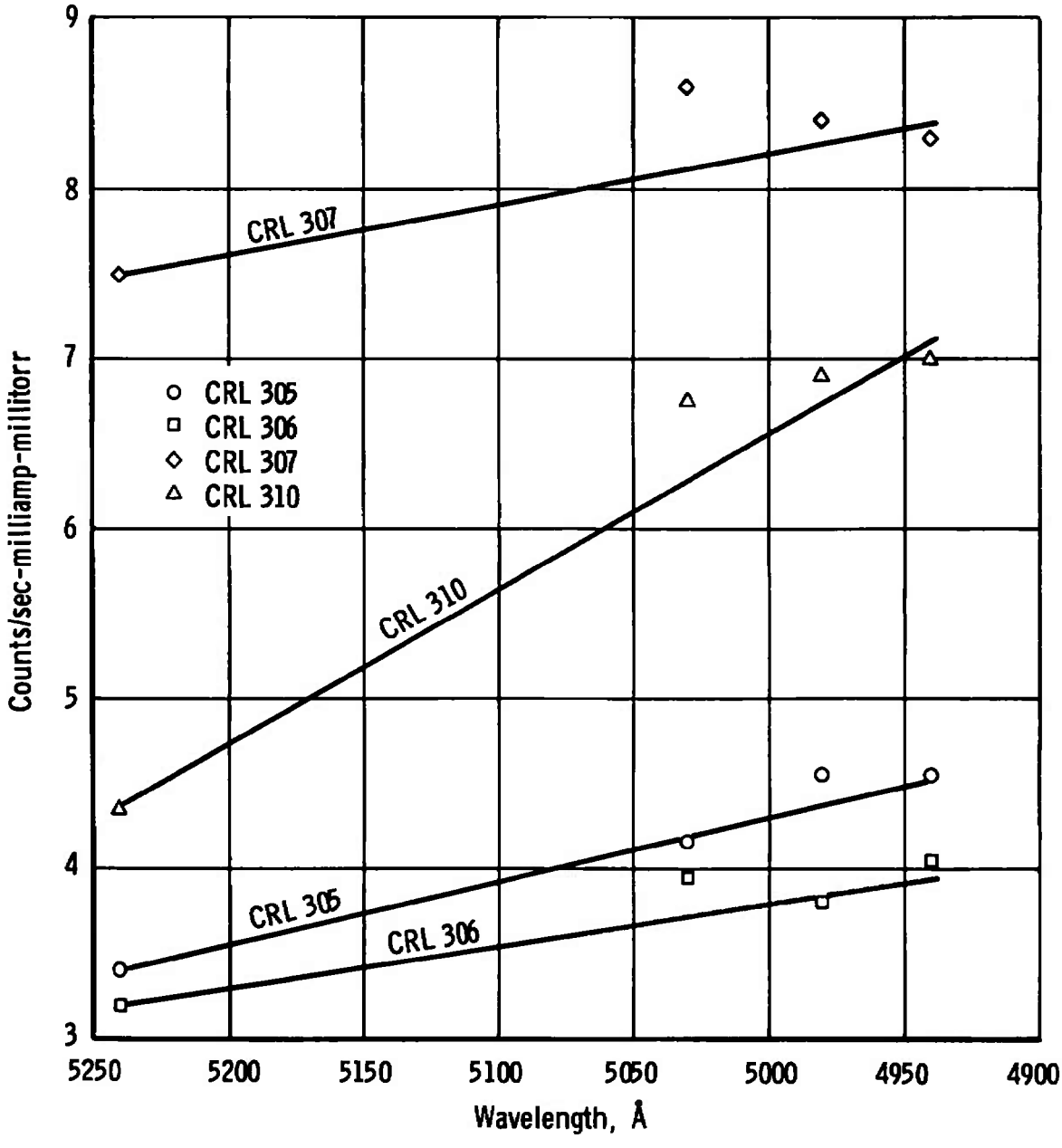

Fig. 25 Lowest Count Rate Points for $\Delta v = -3$ Sequence at 300°K

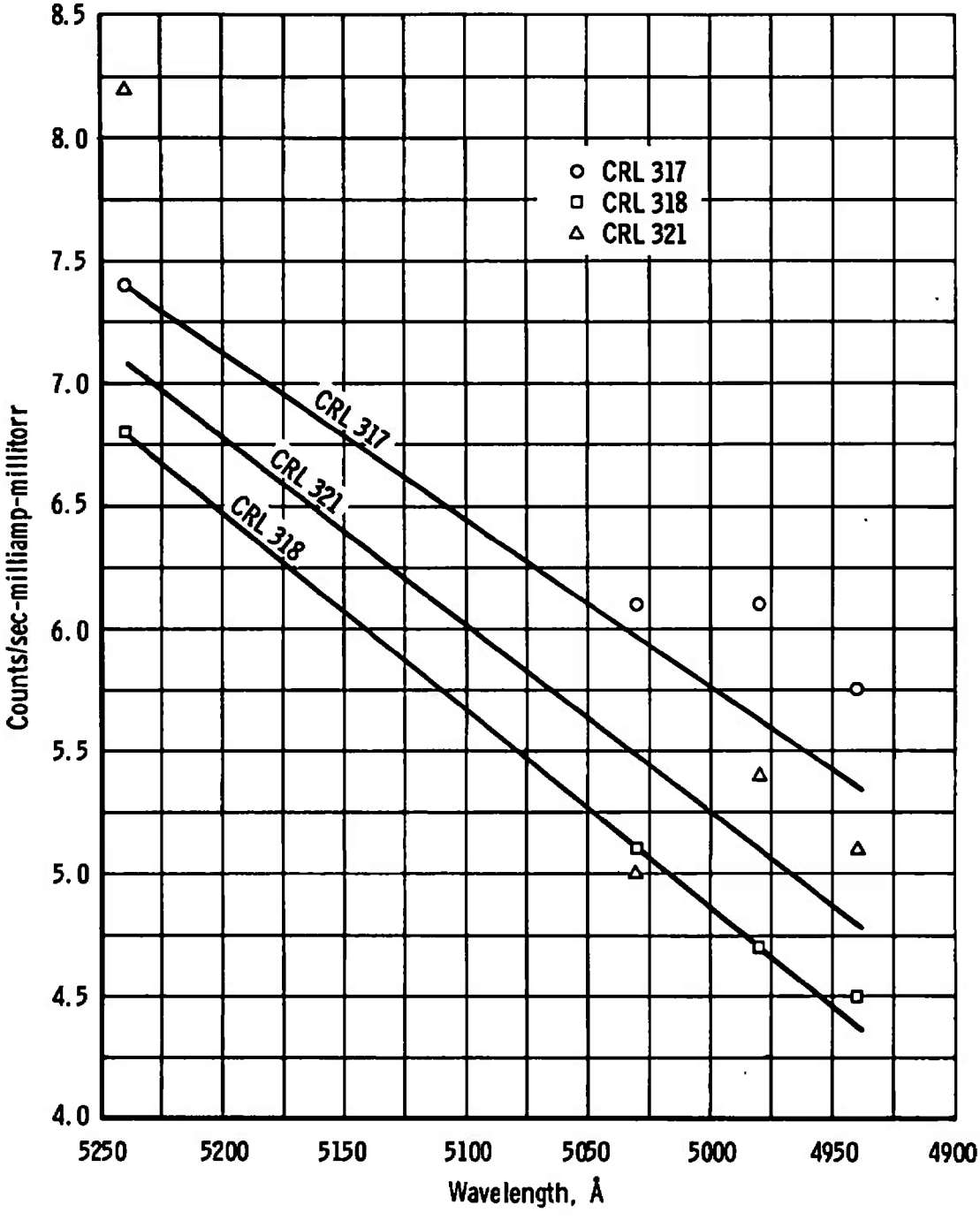

Fig. 26 Lowest Count Rate Points for $\Delta v = -3$ Sequence at 660°K

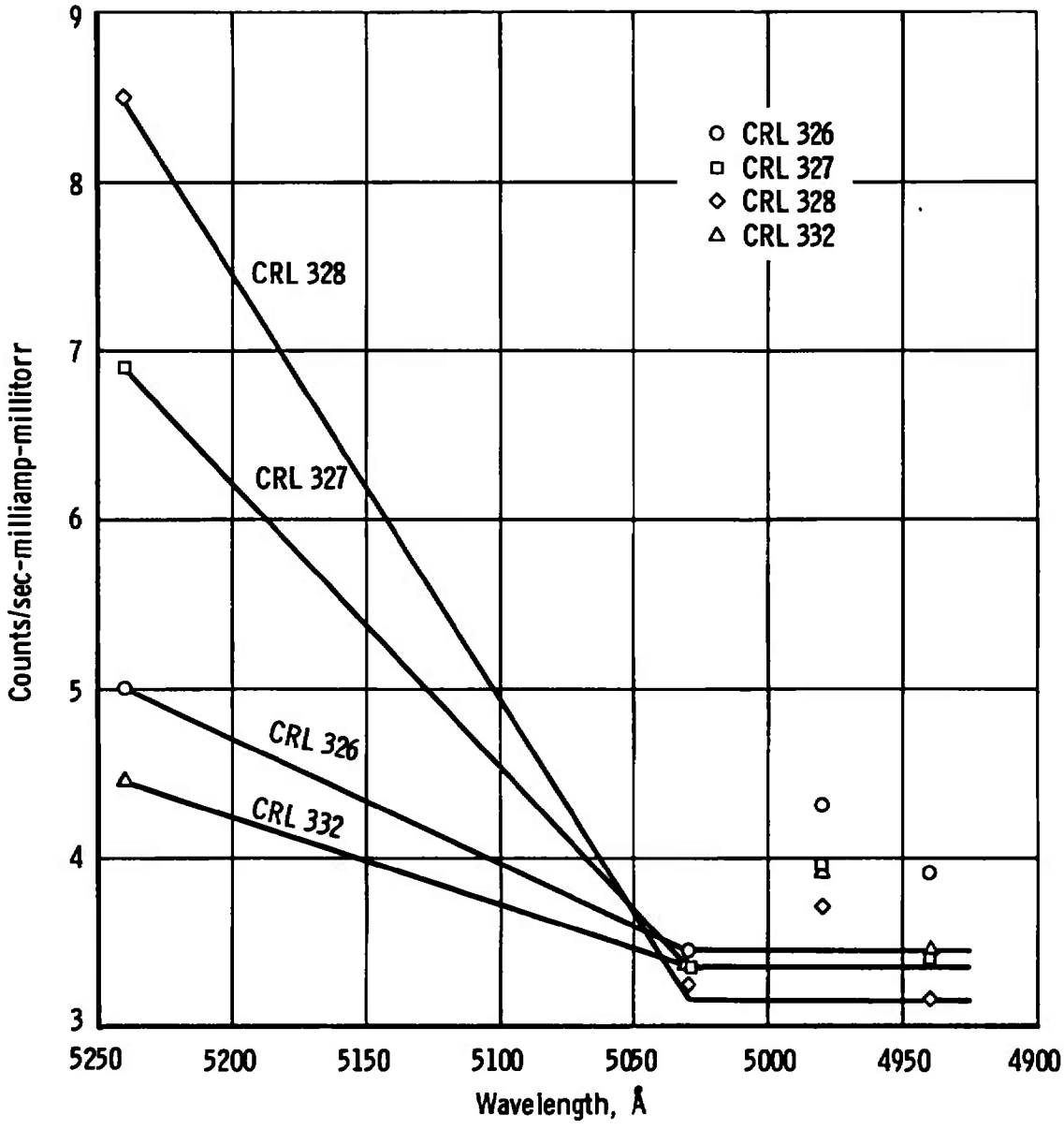

Fig. 27 Lowest Count Rate Points for $\Delta v = -3$ Sequence at 880°K

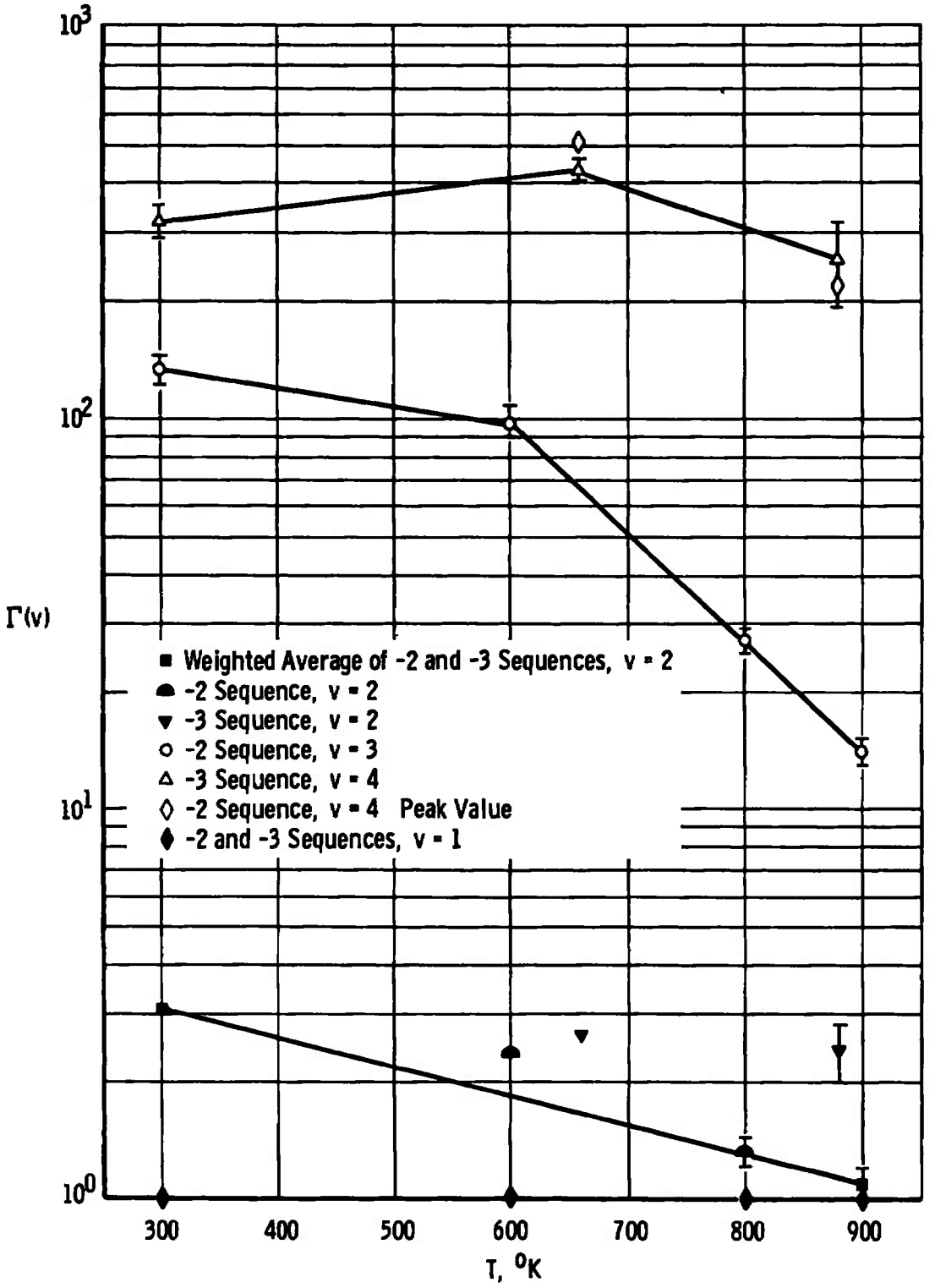

Fig. 28 Enhancement Ratio $\Gamma(v)$ of $N_2^+ B\ ^2\Sigma_u^+(v)$ as a Function of Temperature

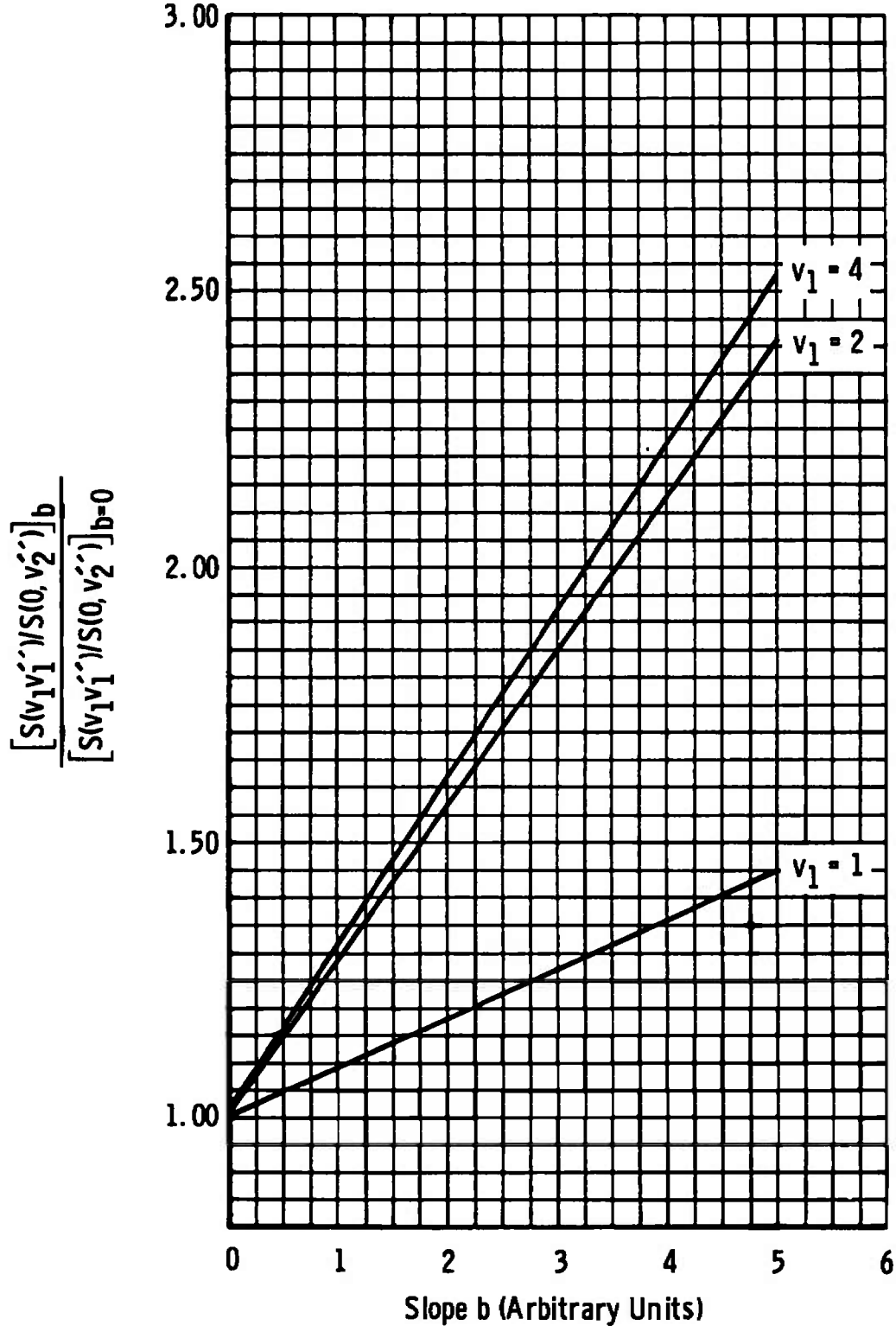

Fig. 29 Variation of Band Intensity Ratio with Slope of Excitation Transition Moment

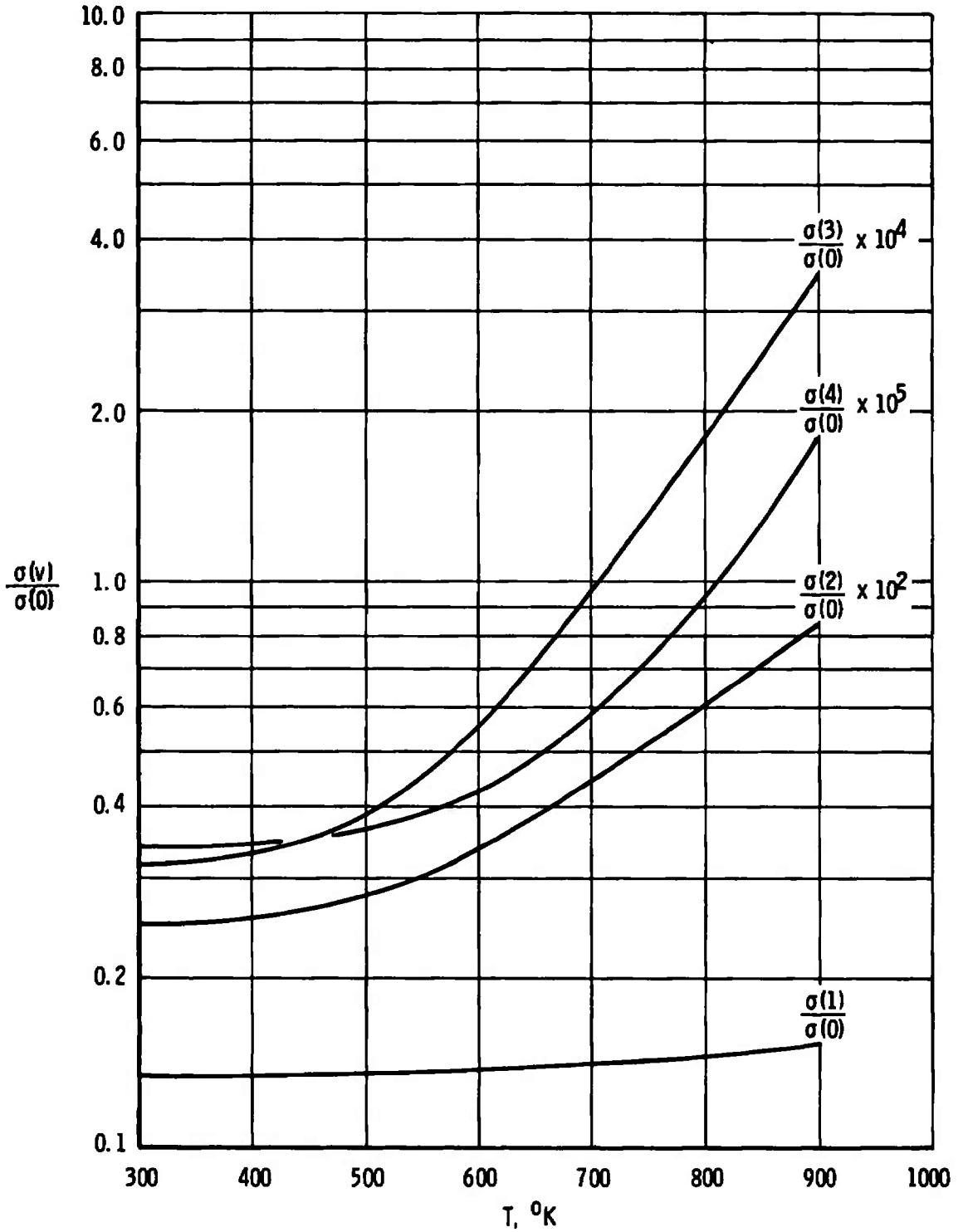

Fig. 30 Excitation Cross Section as a Function of Temperature

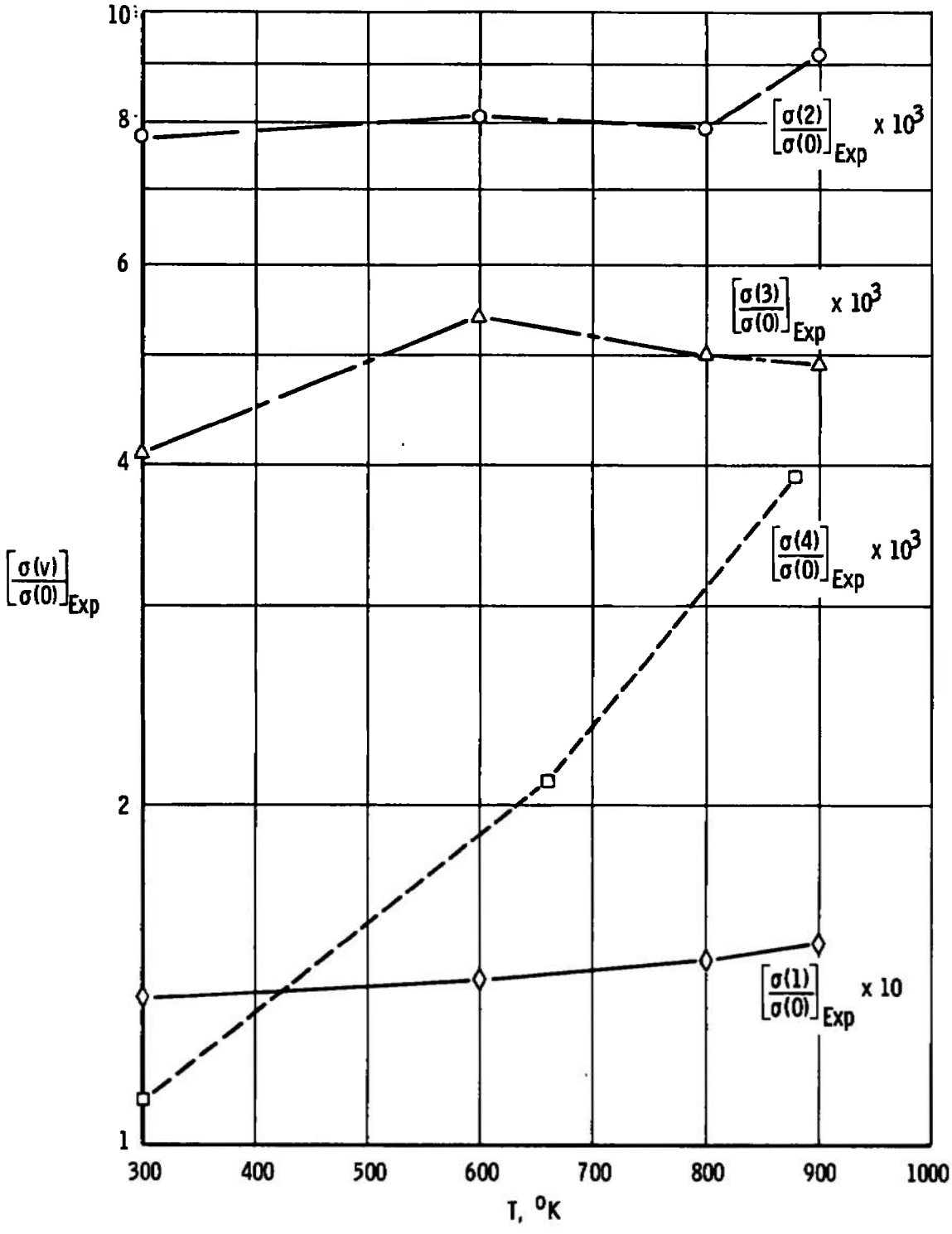

Fig. 31 Experimental Cross-Sectional Ratio $\sigma(v)/\sigma(0)$ as a Function of Temperature

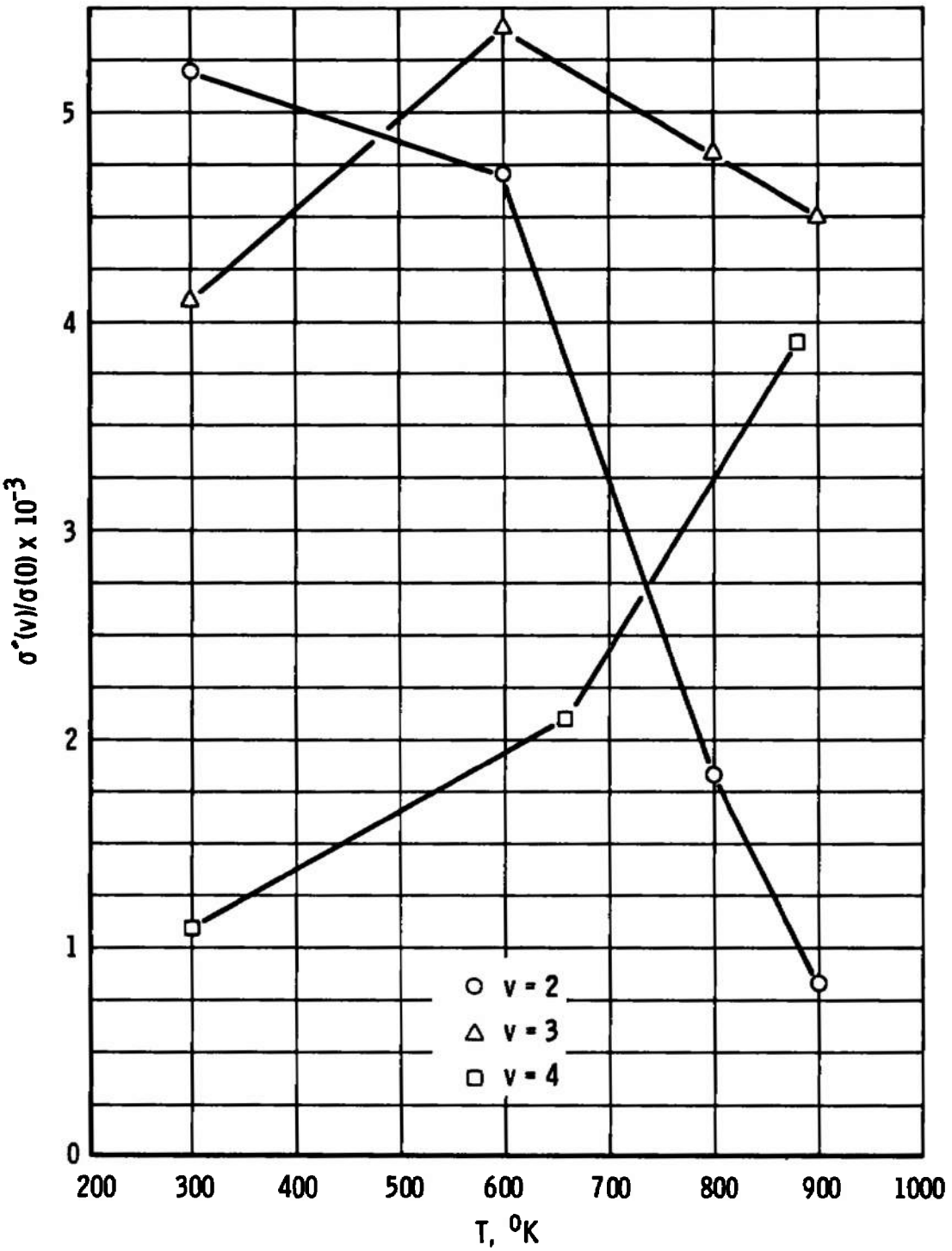

Fig. 32 Cross-Sectional Ratio $\sigma'(v)/\sigma(0)$ as a Function of Temperature

TABLE I
PARAMETERS
a. Emission Parameters

Legend	v'' / v	0	1	2	3	4	5	6	7	8	9
q		6.570(-1)	2.546(-1)	6.858(-2)	1.574(-2)	3.290(-3)	6.374(-4)	1.149(-4)	---	---	
p	0	6.348(-1)	2 706(-1)	7.844(-2)	1.915(-2)	4.230(-3)	8 70(-4)	1.10 (-4)	---	---	
r̄		1.0995	1.0512	1.0128	0.97904	0.9480	0.9170	0.8841	---	---	
q		2.982(-1)	2.316(-1)	2.838(-1)	1.299(-1)	4.182(-2)	1.127(-2)	2.706(-3)	---	---	
p	1	2.580(-1)	2 179(-1)	2.983(-1)	1.472(-1)	5.051(-2)	1.439(-2)	3.640(-3)	---	---	
r̄		1.1523	1.1124	1.0572	1.0177	0.9832	0.9520	0.9222	---	---	
q		4.282(-2)	4.065(-1)	5.608(-2)	2.284(-1)	1.635(-1)	7.010(-2)	2.351(-2)	---	---	
p	2	3.186(-2)	3.452(-1)	5 010(-2)	2.372(-1)	1.836(-1)	8.40(-2)	2.98(-2)	---	---	
r̄		1.2200	1.1611	1.1373	1.0631	1.0227	0.9875	0.9564	---	---	
q		1 954(-3)	1.015(-1)	4.206(-1)	3.688(-3)	1.504(-1)	1.690(-1)	9.324(-2)	---	---	
p	3	1.11 (-3)	7.40 (-2)	3.50(-1)	2.48(-3)	1.58(-1)	1.88(-1)	1.11(-1)	---	---	
r̄		1.3296	1.2289	1.1707	1.2633	1.0688	1 0277	0.9917	---	---	
q		7.592(-6)	5.854(-3)	1 606(-1)	3.973(-1)	3.328(-3)	9.030(-2)	1.544(-1)	1.069(-1)	5.149(-2)	2.008(-2)
p	4	---	3.17(-3)	1 141(-1)	3.22(-1)	4 54(-3)	9 19(-2)	1.70(-1)	1.262(-1)	6 432(-2)	2.639(-2)
r̄		1.7877	1.3476	1.2388	1.1818	0.9145	1.0734	1.0328	0.9956	0.9644	0 9356

TABLE I (Concluded)
b. Excitation Parameters

Legend	v \ v'	0	1	2	3	4	5	6
r_e (Å)	0	8.794(-1)	1.064(-1)	1.269(-2)	1.314(-3)	1.22(-4)	1.0(-6)	---
ω_e (eV)		1.0903	1.0012	0.9520	0.8986	0.8423	0.7676	0.7077
r_e (Å)	1	1.183(-1)	6.876(-1)	1.606(-1)	2.901(-2)	3.982(-3)	4.90(-4)	5.4(-5)
ω_e (eV)		1.1811	1.1000	1.000	0.9540	0.8994	0.8508	
r_e (Å)	2	2.198(-3)	2.012(-1)	5.587(-1)	1.832(-1)	4.559(-1)	7.757(-3)	1.196(-3)
ω_e (eV)		1.3776	1.1916	1.1111	0.9974	0.9575	0.9003	0.7929
r_e (Å)	3	2.8(-5)	4.571(-3)	2.618(-1)	4.747(-1)	1.838(-1)	6.040(-2)	1.120(-2)
ω_e (eV)		0.8433	1.4162	1.2025	1.1239	0.9911	0.9625	0.8579
r_e (Å)	4	2.64(-6)	1.78(-4)	5.528(-3)	3.056(-1)	4.284(-1)	1.680(-1)	7.243(-2)
ω_e (eV)		1.3986	0.9724	1.4813	1.2140	1.1388	0.9782	0.8092

NOTE: Figures in parentheses are exponents of 10; i.e., $6.570(-1) = 6.570 \times 10^{-1}$

TABLE II
LIFETIMES OF $N_2^+ B\ ^2\Sigma_u^+$ VIBRATIONAL LEVELS

	v	0	1	2	3	4
a	$\tau(v)$, 10^{-8} sec	6.58				
b	↓		6.48	6.42	6.43	6.39
c			6.23	5.94	5.72	5.50

LEGEND: a. Result from Ref. 6
b. Results using band strengths
c. Results using Franck-Condon factors

TABLE III
OPTICAL EXCITATION CROSS SECTIONS

	v'' / v'	0	1	2	3	4	5	6	7
a	0	1.00	3.5(-1)	7.1(-2)	1.4(-2)				
b		1.00	3.3(-1)	7.1(-2)	1.3(-2)				
c		1.00	3.0(-1)	6.0(-2)	1.0(-2)				
d		1.00		7.1(-2)	1.3(-2)				
a	1	6.4(-2)	3.9(-2)	4.4(-2)	1.7(-2)	4.2(-3)			
b		---	---	4.9(-2)	1.83(-2)	4.76(-3)			
c		---	---	---	1.50(-2)	3.55(-3)			
d		---	---	---	1.8(-2)	4.8(-3)			
a	2		7.1(-3)		2.9(-3)	---	---		
b			---		---	4.36(-4)	1.52(-4)		
c			---		---	3.47(-4)	1.10(-4)		
d			---		---	8.0(-4)	5.9(-4)		
a	3			3.2(-3)			---		
b				---			5.9(-6)		
c				---			4.53(-6)		
d				---			7.5(-4)		
a	4							---	---
b								6.0(-7)	3.46(-7)
c								4.37(-7)	3.29(-7)
d								---	1.1(-4)

LEGEND: a. Results of Ref. 7
b. Calculated values using emission band strengths
c. Calculated values using emission Franck-Condon factors
d. Present results
NOTE: Figures in parentheses are exponents of 10; i.e., 7.1(-2) = 7.1×10^{-2}

TABLE IV
Δv = -2 SEQUENCE RESULTS

Band Ratio	Temperature, °K	Spectrally Corrected Ratio	4630.54-Å NII Correction Factor	4574.3-Å N_2 (2nd pos) Correction Factor	4601.48-Å NII Correction Factor	4530.40-Å NII Correction Factor	Contaminant-Corrected Ratio	Overlap-Corrected Ratio	Theory
S(13)/S(02)	300	0.262 ± 0.007	0.975	---	---	---	0.256 ± 0.007	0.256 ± 0.007	0.258
	600	0.288 ± 0.008	0.975	---	---	---	0.281 ± 0.008	0.273 ± 0.008	0.264
	800	0.303 ± 0.005	0.975	---	---	---	0.295 ± 0.005	0.280 ± 0.005	0.281
	900	0.317 ± 0.012	0.975	---	---	---	0.309 ± 0.012	0.290 ± 0.012	0.294
S(24)/S(02)	300	0.030 ± 0.001	-	0.70	0.865	---	0.018 ± 0.001	0.018 ± 0.001	6.23×10^{-3}
	600	0.036 ± 0.001	---	0.81	0.865	---	0.025 ± 0.001	0.020 ± 0.001	8.47×10^{-3}
	800	0.040 ± 0.001	---	0.85	0.865	---	0.030 ± 0.001	0.020 ± 0.001	1.52×10^{-2}
	900	0.045 ± 0.001	---	0.86	0.865	---	0.033 ± 0.001	0.022 ± 0.001	2.09×10^{-2}
S(35)/S(02)	300	0.018 ± 0.001	---	---	---	0.61	0.011 ± 0.001	0.011 ± 0.001	8.26×10^{-5}
	600	0.020 ± 0.001	---	---	---	0.69	0.014 ± 0.001	0.014 ± 0.001	1.44×10^{-4}
	800	0.020 ± 0.001	---	---	---	0.68	0.013 ± 0.001	0.013 ± 0.001	4.77×10^{-4}
	900	0.020 ± 0.001	---	---	---	0.67	0.013 ± 0.001	0.013 ± 0.001	8.97×10^{-4}
S(46)/S(02)	Band ratios from P-branch peaks obtained from the three Δv = -2 sequence scans made in the Δv = -3 sequence study were 6.7×10^{-3} at 660°K and 8.1×10^{-3} at 880°K. The theoretical ratios are 1.3×10^{-5} and 3.8×10^{-5}, respectively								

TABLE V
Δv = -3 SEQUENCE RESULTS

Band Ratio	Temperature	Spectrally Corrected Ratio	Overlap-Corrected Ratio	Peak Ratio	Theory
S(14)/S(03)	300°K	0.370 ± 0.008	0.370 ± 0.008	0.336 ± 0.016	0.366
	660°K	0.380 ± 0.018	0.371 ± 0.018	0.361 ± 0.026	0.379
	880°K	0.442 ± 0.058	0.423 ± 0.058	0.425 ± 0.038	0.413
S(25)/S(03)	300°K	0.043 ± 0.004	0.047 ± 0.004	0.036 ± 0.004	0.012
	660°K	0.044 ± 0.001	0.047 ± 0.001	0.048 ± 0.002	0.018
	880°K	0.081 ± 0.016	0.088 ± 0.016	0.065 ± 0.012	0.037
S(47)/S(03)	300°K	0.0074 ± 0.0008	0.0090 ± 0.0008	0.011 ± 0.001	2.8×10^{-5}
	660°K	0.015 ± 0.001	0.018 ± 0.001	0.018 ± 0.002	4.2×10^{-5}
	880°K	0.025 ± 0.008	0.032 ± 0.008	0.028 ± 0.004	1.27×10^{-4}

TABLE VI
RELATIVE APPARENT ELECTRON EXCITATION CROSS SECTIONS AT 300°K

	v	0	1	2	3	4
e	σ(v) Relative	1.00	1.35(-1)	7.8(-3)	3.9(-3)	9.6(-4)
f		1.00	1.18(-1)	9.4(-3)	4.03(-3)	---
e	Γ(v)	---	1.00 ± 0.02	3.1 ± 0.1	130 ± 10	320 ± 30

LEGEND: e. Present results
f. Results from Ref. 7

NOTE: Figures in parentheses are exponents of 10; i.e., 1.35(-2) = 1.35×10^{-2}

UNCLASSIFIED

Security Classification

DOCUMENT CONTROL DATA - R & D

(Security classification of title, body of abstract and indexing annotation must be entered when the overall report is classified)

1 ORIGINATING ACTIVITY (Corporate author)	2a. REPORT SECURITY CLASSIFICATION
Arnold Engineering Development Center, Arnold Air Force Station, Tennessee 37389	UNCLASSIFIED
	2b. GROUP N/A

3 REPORT TITLE

OPTICAL ~~ELECTRON~~ EXCITATION CROSS-SECTION MEASUREMENTS OF THE N_2^+ FIRST NEGATIVE SYSTEM AT ELEVATED TEMPERATURES

4 DESCRIPTIVE NOTES (Type of report and inclusive dates)

Final Report -- May 1971 to May 1972

5 AUTHOR(S) (First name, middle initial, last name)

J. W. L. Lewis, L. L. Price, and H. M. Powell, ARO, Inc.

6 REPORT DATE	7a. TOTAL NO. OF PAGES	7b. NO OF REFS
June 1973	74	12

8a. CONTRACT OR GRANT NO	9a. ORIGINATOR'S REPORT NUMBER(S)
b. PROJECT NO.	AEDC-TR-73-28
c. Program Element 61102F	9b OTHER REPORT NO(S) (Any other numbers that may be assigned this report)
d.	ARO-VKF-TR-72-175

10 DISTRIBUTION STATEMENT

Approved for public release; distribution unlimited.

11 SUPPLEMENTARY NOTES	12. SPONSORING MILITARY ACTIVITY
Available in DDC.	Air Force Cambridge Research Laboratories (SUO), L. G. Hanscom Field, Bedford, Mass. 01730

13 ABSTRACT

Optical electron excitation cross sections of bands of the -2 and -3 sequences of the N_2^+ First Negative System of N_2 were measured over the temperature range from 300 to 900°K. The apparent electron excitation cross sections of the v = 1, 2, 3, and 4 levels, normalized to the v = 0 level, were determined, and enhancement of the experimental values of $\sigma(v \geq 2)$ relative to the predicted values was found for all temperatures investigated. Possible causes of the enhancement and its decrease with increasing temperature are discussed.

3. Optical measurements.

DD FORM 1 NOV 65 1473

UNCLASSIFIED

Security Classification

14. KEY WORDS	LINK A		LINK B		LINK C	
	ROLE	WT	ROLE	WT	ROLE	WT
optical measurement						
electron beams						
electron scattering						
fluorescence						
collision cross sections						
nitrogen						

AFSC
Arnold AFS Tenn